Sediment concentrations and sediment transport in case of irregular non-breaking waves with a current

Part E: Text

May 1992

TU Delft
Delft University of Technology

Coastal Genesis
Rijkswaterstaat

delft hydraulics

G 6 M
MAST

H 840

Sediment concentrations and sediment transport in case of irregular non-breaking waves with a current

F.J. Havinga

CONTENTS

CONTENTS (continued)

CONTENTS (continued)

PREFACE

In 1986 a joint effort of the Delft University of Technology and the Delft Hydraulics, started an experimental program to investigate sediment transport rates.
The objective was to improve experiments for investigation and to get experimental data.
Since then, two programs were executed in a laboratory flume of the Laboratory of Fluid Mechanics. In the first study sand bed material of 200 mu was used. In the second study a similar program was carried out using sand bed material of 100 mu.

Last year, I participated in a third experimental program. The experiments were carried out in a basin of Delft Hydraulics. In this program the influence of a varying current-wave angle was studied. The results of the experiments were compared with the second program (the "earlier 100-mu-study"). Now, the influence of the current-wave angle on a.o. the sediment transport rate became more clear.

For convenience the present report is divided in two parts. Part E contains all text and illustrative figures, part F contains all tables and figures of the experimental data.

Further, I would like to thank the employees of the Delft Hydraulics for their assistance during the execution of the experiments and of course Dr.ir.L.C. van Rijn for his guidance during these experiments, and his advices for interpretation of the experimental results.

F.J. Havinga

May 1992

LIST OF SYMBOLS

a	- reference level	[m]
a(ϕ)	- ϕ-dependent sediment transport coefficient	[-]
Ab	- horizontal orbital displacement amplitude	[m]
B	- coefficient in the Kalinske-Frijlink-Bijker formula	[-]
c	- concentration	[kg/m^3]
c	- time- and bed-averaged concentration	[kg/m^3]
c$'$	- concentration fluctuation	[kg/m^3]
ca	- absolute wave celerity	[m/s]
cr	- relative wave celerity	[m/s]
Dx	- grain diameter exceeded by x%	[m]
Ds	- grain diameter suspended sediment	[m]
fp	- peak frequency	[1/s]
g	- acceleration of gravity	[m/s^2]
h	- water depth	[m]
h0	- water depth relative to the flume bottom	[m]
H	- wave height	[m]
Hsig	- significant wave height	[m]
Ks,ph	- physical bedroughness parameter	[m]
Ks,ap	- apparent bedroughness parameter	[m]
L	- wave length	[m]
L$'$	- wave length relative to the current	[m]
Lb	- bed load	[kg/m^2]
Ls	- suspended load	[kg/m^2]
Lt	- total load	[kg/m^2]
p	- porosity	[-]
q	- power coefficient	[-]
rc	- ripple height in current direction	[m]
rm	- mean ripple height	[m]
rw	- ripple height in wave direction	[m]
s	- standard deviation	[-]
Sb	- bed load transport	[kg/ms]
Scurr	- current-related sediment transport	[kg/ms]
Ss	- suspended load transport	[kg/ms]
Stot	- total load transport	[kg/ms]

LIST OF SYMBOLS (continued)

t	- coordinate of time	[s]
Tp	- wave spectrum peak period	[s]
Tp,rel	- wave spectrum peak period relative to the current	[s]
Tz	- zero-crossing period	[s]
U	- fluid velocity	[m/s]
U	- time- and bed-averaged fluid velocity	[m/s]
U´	- fluid velocity fluctuation	[m/s]
Ub	- horizontal orbital velocity amplitude	[m/s]
Um	- depth-averaged fluid velocity	[m/s]
U*	- shear velocity	[m/s]
U*,c	- shear velocity by current	[m/s]
U*,w	- shear velocity by waves	[m/s]
Wss	- fall velocity suspended sediment	[m/s]
x,y,z	- length coordinates	[m]
y	- power coefficient	[-]
Z+	- reference level relative to mean bed level	[m]
z0	- zero velocity level	[m]
z1	- adapted zero velocity level	[m]
β	- ratio of sediment and fluid mixing coefficient	[-]
γ	- apparent roughness increase coefficient	[-]
Δ	- relative sediment density	[-]
δ	- mean bed level	[m]
δb	- mixing layer	[m]
η	- water surface elevation	[m]
ϕ	- current-wave angle	[°]
κ	- constant of Von Karman	[-]
λc	- ripple length in current direction	[m]
λm	- mean ripple length	[m]
λw	- ripple length in wave direction	[m]
$\lambda 1$	- upstream ripple length	[m]
$\lambda 2$	- downstream ripple length	[m]
μ	- mean value	[-]
ν	- kinematic viscosity	[m^2/s]
ρ	- correlation coefficient	[-]
ρs	- density of sediment	[kg/m^3]
ρw	- density of fluid	[kg/m^3]

1. Introduction

Many coastal engineering problems are related to transports of sediment. For prediction of coast-lines in the future, the prediction of the net sediment transport is essential. Various models, such as that of Bijker, Van Rijn, Nielsen, Engelund & Hansen, and Ackers & White are available to predict the sediment transport, by knowledge of wave height and current-strength. The reliability of these models is unknown, because data under field conditions are scarce. Only few relations between sediment transport, current velocity and wave height are known.
For these reasons a laboratory study was carried out to extend the knowledge of the basic phenomena in morphological processes. The study contains experiments in which sediment concentrations and fluid velocities have been measured in case of irregular non breaking waves alone, in combination with waves under an angle ϕ (current-wave angle), and in case of current alone.

The present report contains a description of an experimental program, as a follow up of experiments by v.d. Kaaij and Nieuwjaar in 1986, and Nap and Van Kampen in 1987. As in the second study, in the present study a particle sand diameter of D50 = 100 mu was used, so that the experiments of Nap and Van Kampen will be referred as "the earlier 100-mu-study". The results of that study will be compared with the present results. Because of the fact that the sediment transport rate is studied for varying current-wave angles, it was not possible, in contradiction with the earlier studies, to execute the experiments in a flume. Therefore the program was carried out in a basin of Delft Hydraulics.

In chapter 3 the experimental set up (measuring instruments, experimental program) will be described. In chapter 4 the methods for estimating the several parameters (sediment transport, ripple parameters) will be described, the experimental results will be discussed.
In chapter 5 the bed roughness and its relationship to concentrations and velocities in the near bed zone will be discussed. A comparison between the measured sediment transport rates and the predicted values by Van Rijn and Bijker is made. Finally, in chapter 7, a list of conclusions and recommendations is presented.

To explain the objective of the experiments in the present study, some basic theory of sediment transport processes will be described in the next chapter.

2. Sediment transport computation

2.1 Sediment transport basics

The computation of the sediment transport rate can be done by multiplying the sediment concentration distribution over the water depth with the sediment velocity. The sediment concentration over the depth is caused by stirring up of sediment particles from the sand bed. The stirring up process is induced by wave and current movements in the near bed zone.

Assuming that the sediment velocity is equal to the fluid velocity, the sediment transports can be computed from:

$$Sy(x,y,t) = \int_{0}^{h(x,y)+\eta(x,y,t)} c(x,y,z,t) * Uy(x,y,z,t)\, dz \qquad (1.1)$$

$$Sx(x,y,t) = \int_{0}^{h(x,y)+\eta(x,y,t)} c(x,y,z,t) * Ux(x,y,z,t)\, dz \qquad (1.2)$$

with:

Sy (x,y,t)	= Local instantaneous sediment transport rate per unit width in long-shore direction	[kg/sm]
Sx (x,y,t)	= Local instantaneous sediment transport rate per unit width in cross-shore direction	[kg/sm]
c(x,y,z,t)	= Local instantaneous sediment concentration	[kg/m³]
Uy (x,y,z,t)	= Local instantaneous y-component of the fluid velocity	[m/s]
Ux (x,y,z,t)	= Local instantaneous x-component of the fluid velocity	[m/s]
x	= Horizontal coordinate, cross-shore	[m]
y	= Horizontal coordinate, long-shore	[m]
z	= Height above mean bed level	[m]
t	= Time	[s]
η	= Water surface elevation	[m]
h(x,y)	= Water depth	[m]

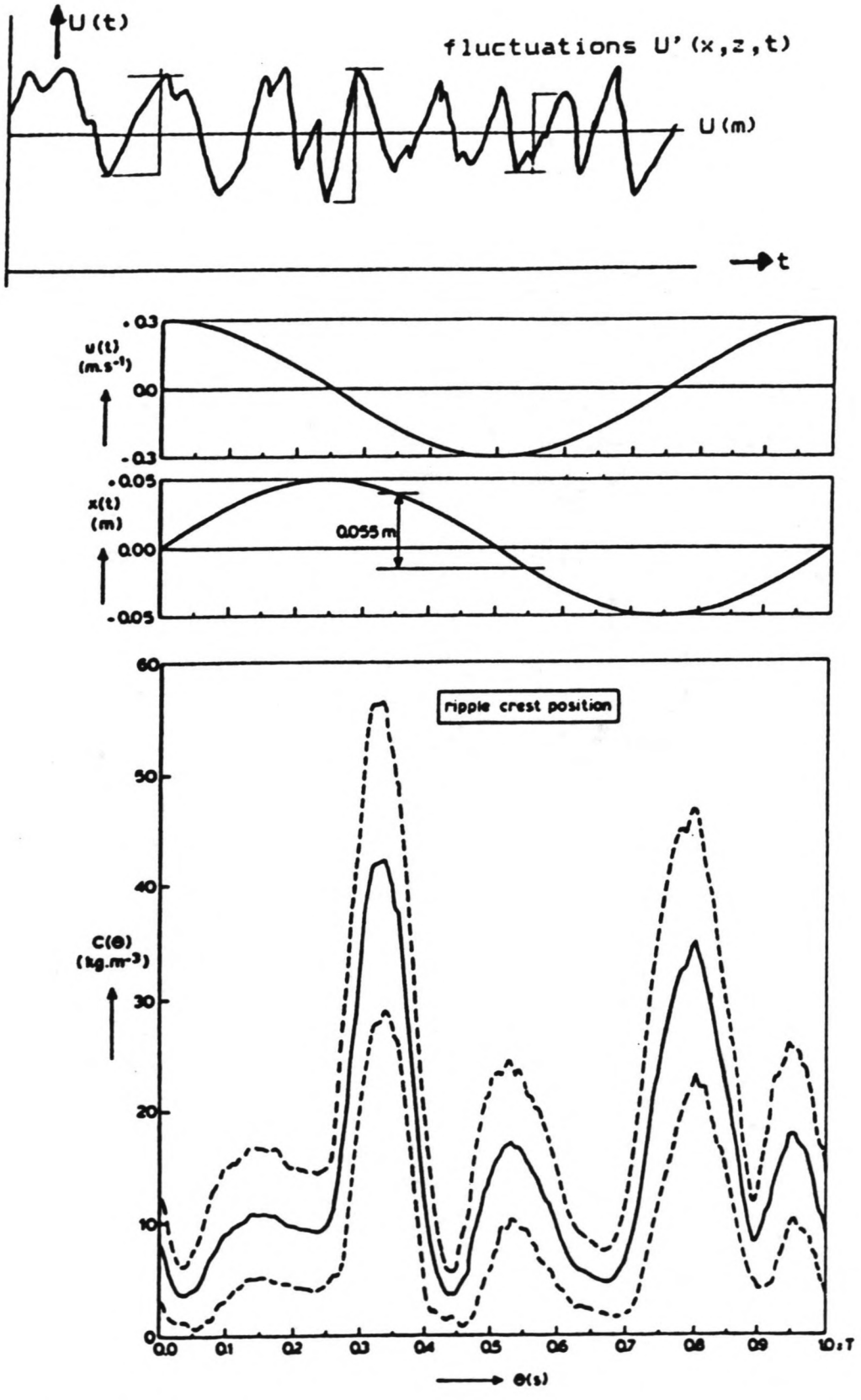

Figure 1B Ensemble mean and standard deviation of concentration in single period

Measuring instantaneous fluid velocity and sediment concentration is quite difficult. Bosman (1985) investigated the concentration as a function of time. The concentration c(z,t) was measured within a wave period, at a fixed point about 3 cm above mean bed level. Fig.1b shows ensemble mean concentrations based on averaging over 99 periods and standard deviations. Based on the random scatter of the concentrations, it is obvious that Bosman concluded that it is not practical to relate the instantaneous concentrations to the instantaneous fluid velocities.

In these experiments both instantaneous concentrations and instantaneous velocities were measured. In the present study the computations are all based on averaged values.
This implies that a part of the total sediment transport is neglected as is shown below.

Defining : $c(x,y,z,t) = \overline{\overline{c}}(y,z) + c'(x,y,z,t)$ (1.3)

$Uy\ (x,y,z,t) = \overline{\overline{Uy}}(y,z) + Uy'(x,y,z,t)$ (1.4)

$Ux\ (x,y,z,t) = \overline{\overline{Ux}}(y,z) + Ux'(x,y,z,t)$ (1.5)

with:

$\overline{\overline{c}}(x,z)$ = Time- and bed-averaged component of the local instantaneous concentration.

$c'(x,y,z,t)$ = Fluctuating component of the local instantaneous concentration.

$\overline{\overline{Uy}}(y,z)$ = Time- and bed-averaged component of the local instantaneous fluid velocity in y-direction.

$\overline{\overline{Ux}}(y,z)$ = Time- and bed-averaged component of the local instantaneous fluid velocity in x-direction.

$Uy'(x,y,z,t)$ = Fluctuating component of the local instantaneous fluid velocity in y-direction.

$Ux'(x,y,z,t)$ = Fluctuating component of the local instantaneous fluid velocity in x-direction.

The fluctuating components are caused by:

- orbital fluid movements, induced by the waves, and
- fluctations in the main flow.

Turbulence and the irregularity of waves will increase this effect.
See Fig.1a and 1b.

Substituting Eqs. (1.3) and (1.4) into Eq. (1.1)
leads, to :

$$Sy(x,y,z,t) = \int_0^{h(x,y)+\eta(x,y,t)} c(x,y,z,t)*Uy(x,y,z,t)dz =$$

$$\int_0^{h(x,y)+\underline{\eta}(x,y,t)} \underline{\underline{c}}(y,z)*\overline{\overline{Uy}}(y,z)dz + \int_0^{h(x,y)+\eta(x,y,t)} c'(x,y,z,t)*\overline{\overline{Uy}}(y,z)dz +$$

$$\int_0^{h(y)+\underline{\eta}(y,t)} \underline{\underline{c}}(y,z)*Uy'(x,y,z,t)dz + \int_0^{h(x,y)+\eta(x,y,t)} c'(x,y,z,t)*Uy'(x,y,z,t)dz \qquad (1.6)$$

Comparable relations are found for Sx(x,y,z,t).
Averaging over time and bed (in x-direxion), the total sand transport, is defined as:

$$Sy\ (y) = \overline{\overline{Sy}}(x,y,t) \qquad (1.7)$$

$$Sx\ (y) = \overline{\overline{Sx}}(x,y,t) \qquad (1.8)$$

And substitution of Eq. (1.6) into Eq. (1.7) yields:

$$Sy\ (y) = \int_0^{h(y)} \overline{\underline{c}}(y,z)*\overline{\overline{Uy}}(y,z)dz + \int_0^{h(y)} \overline{c'}(x,y,z,t)*\overline{\overline{Uy}}(y,z)dz +$$

$$\int_0^{h(y)} \overline{\underline{c}}(y,z)*\overline{Uy'}(x,y,z,t)dz + \int_0^{h(y)} \overline{c'}(x,y,z,t)*\overline{Uy'}(x,y,z,t)dz$$

$$Sy\ (y) = \int_0^{h(y)} \underline{\underline{c}}(y,z)*\overline{\overline{Uy}}(y,z)dz + \int_0^{h(y)} c'(x,y,z,t)*Uy'(x,y,z,t)dz$$

and for x-direction:

$$Sx\ (y) = \int_0^{h(y)} \underline{\underline{c}}(y,z)*\overline{\overline{Ux}}(y,z)dz + \int_0^{h(y)} c'(x,y,z,t)*Ux'(x,y,z,t)dz \qquad (1.9)$$

The final result of Eq.(1.8) shows that the total sediment transport is devided into two parts:
The first part is determined by time- and bed-averaging. It represents the transport of sediment by U(z), as if there is a steady current. Therefore this part of the sediment transport is defined as the current-related sediment transport.
The second part of the sediment transport is mainly caused by the orbital movements, U(x,y,z,t), effected by the irregular waves. So this part is called the wave-related sediment transport.
(These terms were also used in the earlier 100-mu-study, in the 200-mu-study the parts were called respectively convective and diffusive part.)

Eq.(1.9) is a useful approximation of Eq.(1.1). For the current-related sediment transport it is sufficient to measure time- and bed averaged velocities and concentrations.
In both this study and the earlier 100-mu- and 200-mu-study it resulted in an estimation of the current-related sediment transport. To investigate the relative importance of the wave-related sediment transport, the instantaneous values of concentration and fluid velocity were measured with the Acoustical Sediment Transport Meter (ASTM) and the Electro Magnetical Fluid velocity meter (EMS or EMF),(see chapter 3).

2.2 Long-shore and cross shore sediment transport

Waves approaching a coast, will reach the coast under a small angle, caused by refraction. The radiation stress, generated by the waves under a small angle, and bottom friction stresses, result in a longshore current.
Fig.2 shows two cross sections, in which two different morphological processes are present.

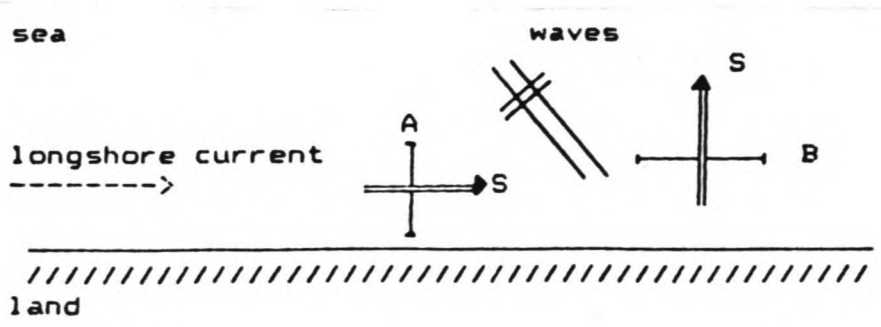

Figure 2 Longshore and cross-shore sediment transport

The sediment transport in cross-section A represents a longshore sediment transport. This is stirring up of sediment, by waves and current, transported by a rather steady longshore current.(wave-induced and/or tide-induced). Through cross-section B, a cross-shore sediment transport is present. In this case, the velocity oscilliations $U'(x,y,z,t)$, introduced by orbital movements, do strongly influence the transport of sediment, during a wave period.

The longshore sediment transport is assumed to be represented by the current-related part of the total sediment transport (see Eq.(1.9)):

$$Sy\ (y) = \int_0^{h(y)} c(y,z) * \overline{\overline{Uy}}(y,z)\ dz \qquad (1.10)$$

This because of the fact that fluid velocity does not depend on time (the longshore current is rather constant at each point above the mean bed level), and because the time- and bed-averaged concentration c(z) can be measured with reasonable accuracy.

For cross-shore sediment transport, this simplification (Eq. 1.10) is not allowed. The parameter Ux(y,z,t) and the parameter c(y,z,t) do strongly depend on time. In this case, the wave-related sediment transport plays a much more important role than in the longshore transport computations.

In the earlier 100-mu-study the relation between current and waves, in same or opposite direction, and the sediment transport was investigated. In the present study the influence of the current-wave angle on the sediment transport rate is investigated. The experiments were carried out with current- wave angles of ϕ=90°, ϕ=60° and ϕ=120°.
In all experiments time- and bed-averaged velocities were measured. In some tests the instantaneous values of the concentrations (ASTM) and velocities (EMS) were recorded in the computer, to investigate the importance of the wave-related sediment transport. An estimation of the cross-shore sediment transport can be made now.

2.3 Objective of the present experiments

1. Identification of the relationship between current-related sediment transport, wave height and current velocity, and comparison with the earlier 100-mu-study.

2. Investigation of the influence of the current-wave angle on the current-related sediment transport parameters.

3. Verification of the Bijker model and the van Rijn model for the current-related suspended sediment transport.

4. Investigation of effective bed-roughness of wave- and current-induced ripples.

5. Investigation of the wave-related part of the sediment transport rate and the cross-shore sediment transport. (Not presented in this report.)

3. Experimental set up

3.1 The Vinje basin

A. Description of the physical model

Figure 3 shows a plan view (see also photo 1) of the physical model:

1. wave height meters
2. gauging stations
3. inflow tubes
4. measuring carriage
5. grain bottom
6. grid with variable openings

The waves are generated by the wave generators and are reaching the channel under an angle (ϕ). The gravel slope of 1:8 damps almost the total wave energy (no reflection). In the basin wave height meters (1.) are placed as well in the "wave-section" as in the channel. The gauging stations (2.) are placed near the inflow- and outflow section.
The inflow section exists of three inflow tubes (3.), which can, depending on the desired current strength, all be opened. The rigid bottom section (5.) and the grid (6.) provide that an uniform velocity distribution over the width of the channel is generated. The guiding plates guide the current, with a minimum of loss of discharge, in the channel.
The measuring carriage (4.) is situated above the channel (width of 4 meter), and can moved over a rail (see photo 2,3). The carriage is always placed as far away as possible from the disturbing zones (inflow-, outflow sections etc., see under D. Test section).

B. Wave generation

The irregular waves are generated by the irregular movements of a series of individually-steered wave paddles (see Fig.3). The desired wave spectrum is created by a computer file. The spectrum is single topped, with a peak frequency of 0.4 Hz and a JONSWAP-form (see also Fig.7). The wave height is controlled by an amplifier.

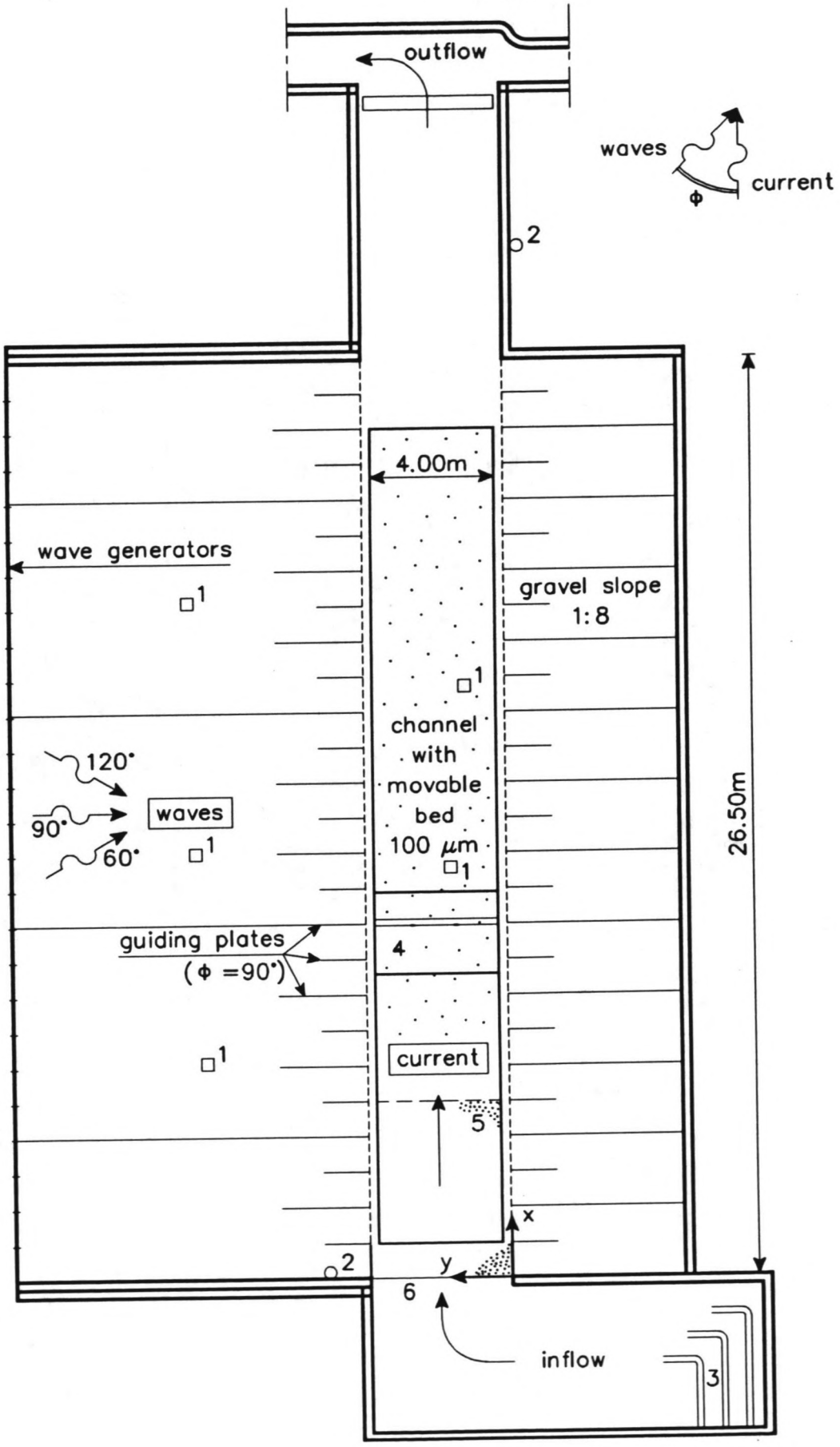

Figure 3 Plan view of wave-current basin

In this basin it is possible to generate waves under different angles to the channel. This angle was generated by a certain wave motion of the paddles, starting at section 1 (see Fig.4, photo 8).

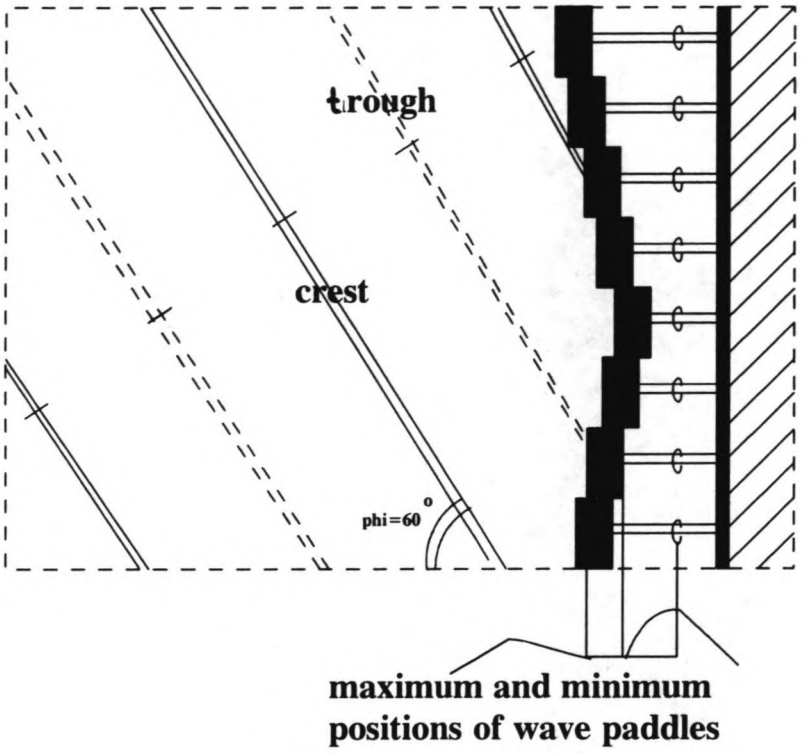

Figure 4 Generation of waves under an angle.

C. Current generation

The discharge was generated by a pump system. Every pump has a discharge of about 200 m3/s. By opening a number of pumps it was possible to generate several current strengths in the basin. In the test period before the experiments were carried out, the influence of the guiding plates in the basin on the current was studied. The guiding plates give an extra turbulence, but it was not known in what way the plates would effect the (velocity and concentration) measurements.

Therefore, the velocities were measured over the width of the channel. By using a grid with variable openings at the inlet, it was possible to create a uniform velocity profile over the channel. The results of two of those tests are presented in Table 1 and Table 2. (y=distance across channel width, Um=average velocity in the channel)

Photo 1, wave and current basin
waves normal to current

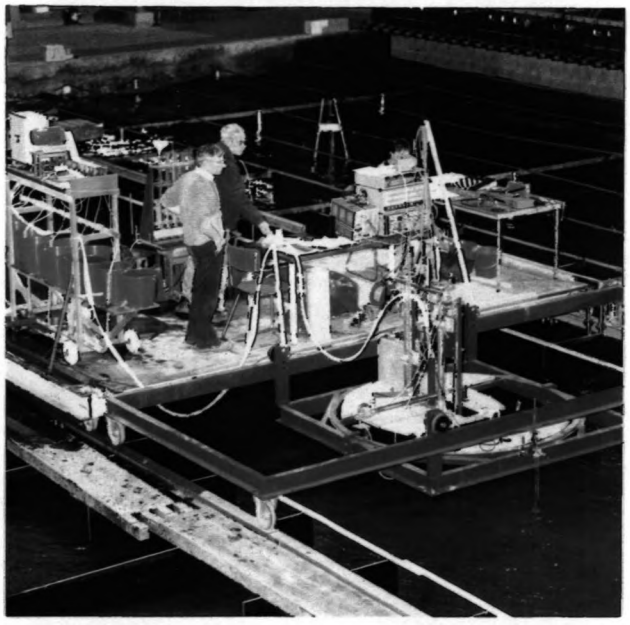

Photo 2, measuring platform

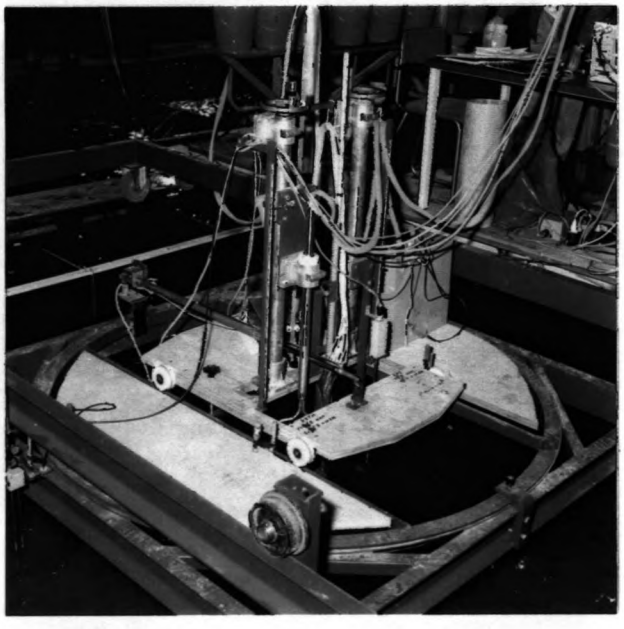

Photo 3, measuring carriage with
instruments

Photo 4, acoustical velocity and
concentration probe (left)
pump intakes (middle)
electro magnetic velocity
probe (right)

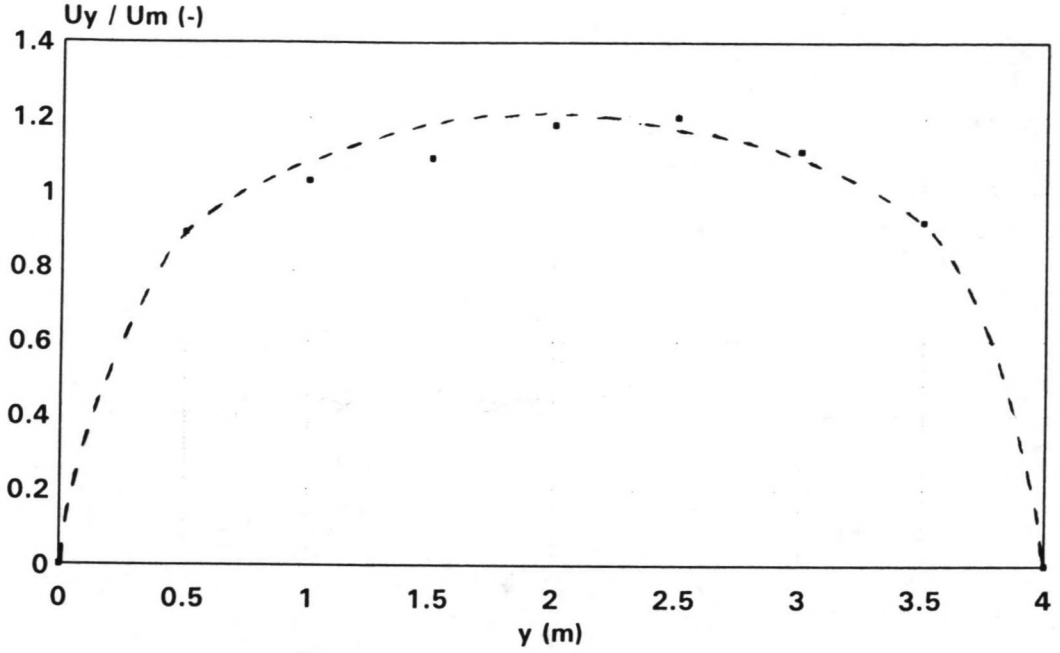

Figure 5A Velocity distribution over the width of the channel

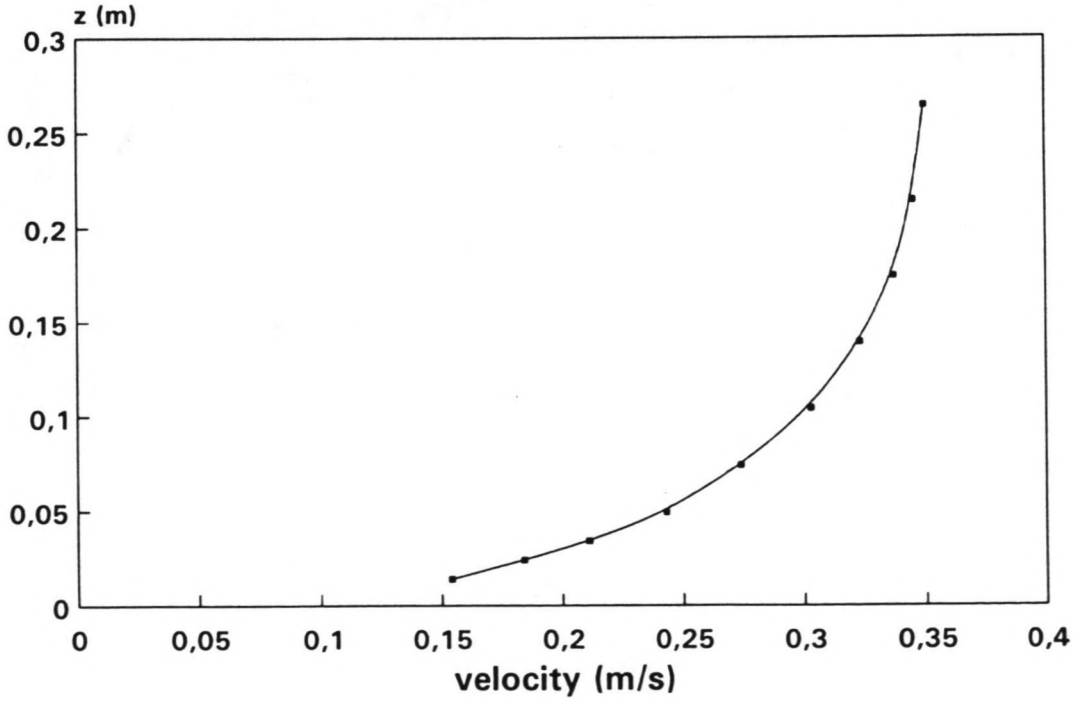

Figure 5B Logarithmic velocity distribution

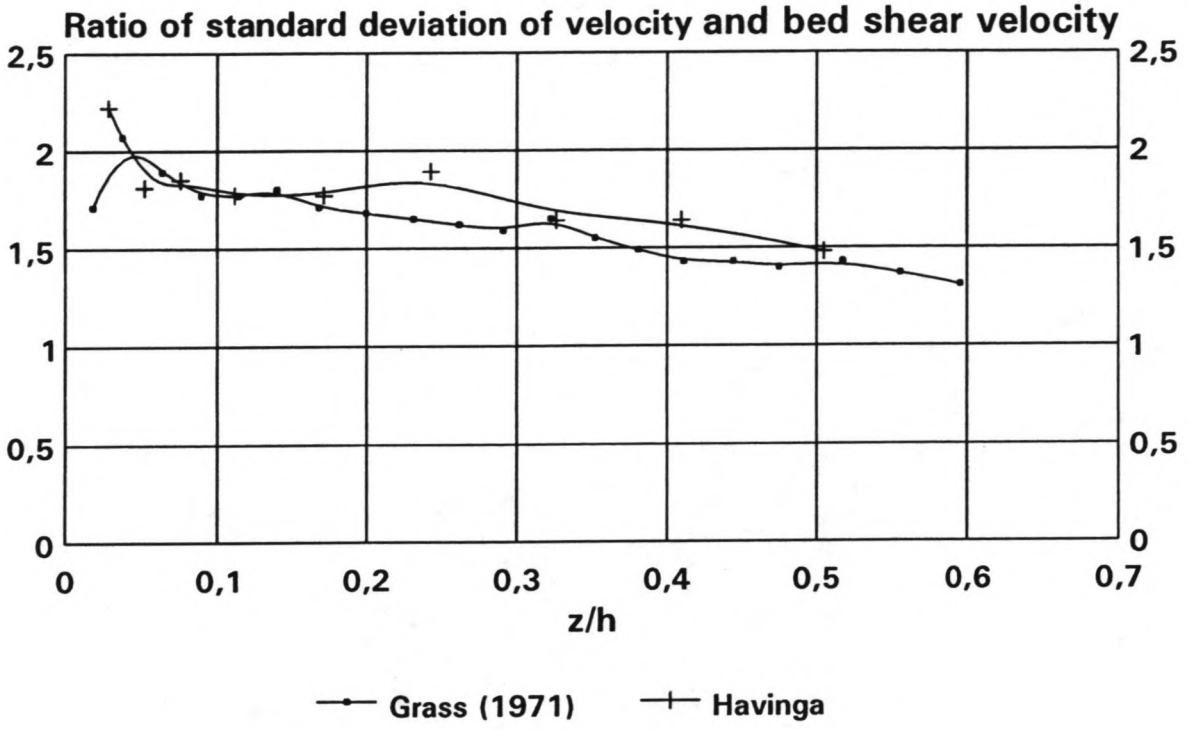

Figure 5C Relative turbulence intensity

y(m)	0.5	1.0	1.5	2.0	2.5	3.0	3.5
test 1	21.0	25.0	25.5	26.0	25.5	25.0	22.5
test 2	27.5	36.0	41.5	39.0	34.0	30.5	34.0

Table 1 Mean velocities (cm/s) over the width

y(m)	0.5	1.0	1.5	2.0	2.5	3.0	3.5
test 1	0.93	1.10	1.12	1.15	1.12	1.10	0.99
test 2	0.85	0.95	1.06	1.21	1.29	1.12	0.85
mean t1,t2	0.89	1.03	1.09	1.18	1.20	1.11	0.92

Table 2 Ratio U(y)/Um over the width

In these tests the velocities were measured 5 times for a period of 30 seconds. From the Tables 1 and 2 it is clear that the velocity distribution is rather uniform over the width of the channel (see Fig.5). Tests at other locations in the channel gave comparable results. Further, float track

measurements showed straight lines along the channel. As is shown in chapter 4 and 5, the velocity profiles over the depth could be very well described by a logarithmic distribution. See also Figures 5.3.A-I.
Figure 5C shows relative turbulence intensity over the depth for current velocity of 0.3 m/s. Good agreement with other data (Grass, 1971) can be observed.
From these test results it was concluded that the guiding plates don´t generate much extra turbulence, so the plates will not effect the measurements significantly.

Using one pump of the pump system, an average current of approximately 12 cm/s was generated. By using two pumps the average current was about 24 cm/s. The third current condition, an average current of 30 cm/s, was generated by using three pumps. A permanent overflow weir, situated at the end of the channel (see Fig.3), is used to controll the water level. The height of this weir did not vary more than one centimeter (2.5%), under same pump conditions. So the generated discharge didn´t vary much .

D. Test section

Water entering the channel via the pump system had no initial sediment load; the concentration had to build up completely in the section with the sand bed. The sand bed had a thickness of about 0.10 m. To provide enough length to reach equilibrium concentrations over the depth, the test section for ϕ=90° was located at section 18 meter (approximately 30 times the waterdepth). For waves approaching under an angle of ϕ=60° and ϕ=120° it appeared that the wave generator couldn´t create a uniform wave height over the channel length. The waves reflected via the basin wall were interfering each other. It was necessary to select the test section as far away as possible from the disturbing zone. For ϕ=60° the test section was located at section 20 meter, and for ϕ=120° at section 15 meter. (see also Fig.3).
During the experiments under a current-wave angle of 120°, the measured wave height was observed to be inaccurate. Therefore the steering file for the experiments T 14 20 and T 14 30 were changed. The waves were not reflected via the wall anymore. The result was that the wave height was more uniform now, but the velocities, compared to the former experiments, didn´t seem very reliable anymore. (The velocities near the bottom were relatively high, see also section 5.7.)

3.2 Sediment

The sediment that was used in the present study, just as in the earlier 100-mu-study, is called "Asser sand". After each experiment, a bed material sample was taken at the test section. By sieving the samples, the characteristics of the bed material were determined. The values of D10, D50 and D90 are given in Table 3, minimum and maximum values are presented over the experimental period.

Dx	D10	D50	D90
mean [mu]	70	100	130
minimum [mu]	59	89	121
maximum [mu]	76	107	145

Table 3 min, max and mean Dx values in the measuring section, during the study.

Because of the fact that the sediment was brought in suspension by wave movement and transported over the weir, there was a loss of (most fine) material. At regular times the sand bed was resupplied and mixed.

3.3 Measuring instruments and methods

The following instruments, with the parameters that were measured during the experiments, will be discussed:

- Mean bed level
- Water level
- Wave parameters and spectrum
- Time- and bed-averaging
- Sediment concentration measurements
- Water velocity measurements
- Ripple parameters
- Particle diameters of bed material
- Fall velocity
- ASTM measurements

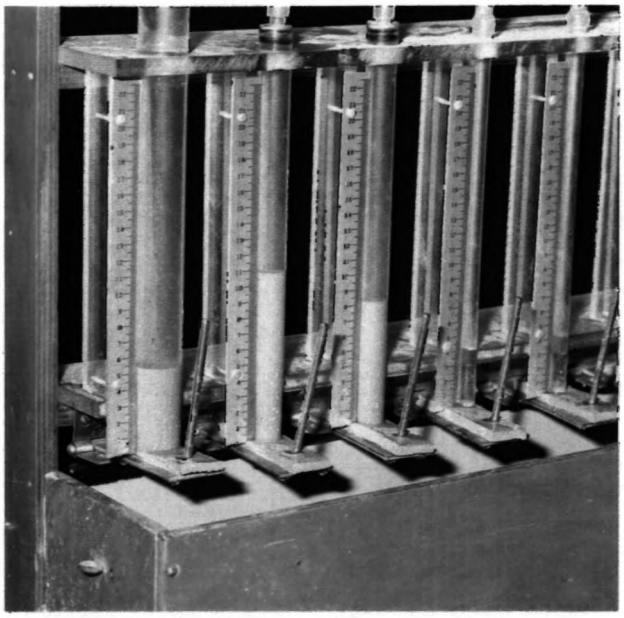

Photo 5, calibrated volume meter (sand concentrations)

Photo 6, pump equipment

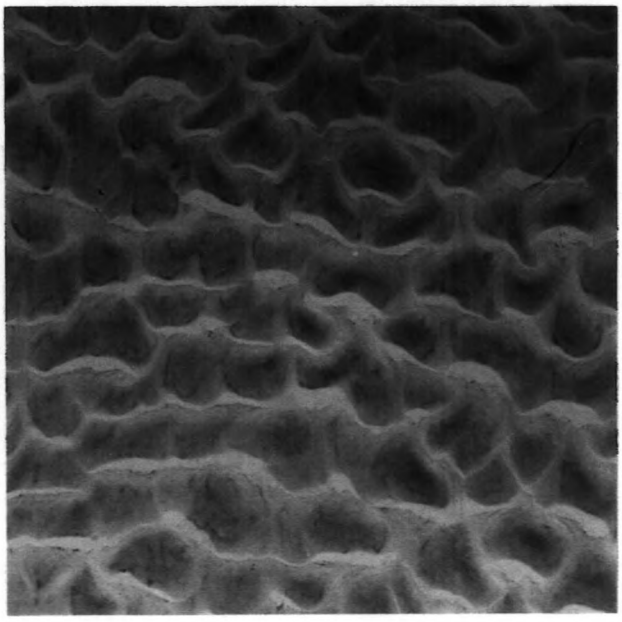

Photo 7, ripple pattern, waves normal to current

Photo 8, waves oblique to current

3.3.1 Mean bed level

To determine the mean bed level δ in the measuring section, a profile follower (profo) and an integrator were used. Both instruments were mounted on the moving measuring carriage (see section 3.3.4.). During the time the profo measures, over a zone of two times 65 cm (perpendicular to the current direction), the electronical output of the profo is integrated, and averaged by a mean value meter. The MVM gives the mean value of δ, the distance between the mean bed level and a chosen reference level ("zero level"). Because of the fact that the mean bed level could change during the experiment, δ was determined six times during one experiment.

3.3.2 Water level

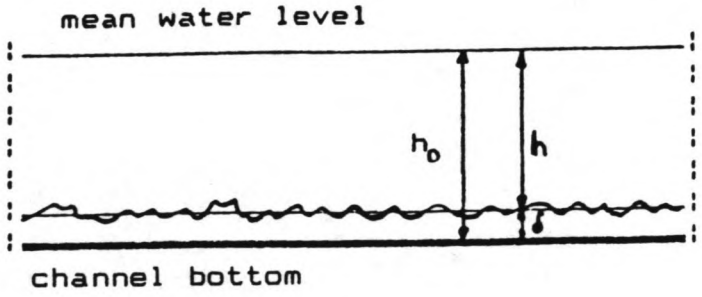

Fig. 6 Mean bed level and mean water depth.

The water level was measured at two points in the model. One gauging station was situated near the inflow section, the other at the end of the flume (see Fig.3). The two measured values, each test one measurement, were averaged. During one experiment the mean water height didn't change for, according the gauging stations, more than one millimeter. Both stations were also related to the zero-level, so the water height relative to the mean bed level, h, can be determined as:

$$h = h0 - \delta$$

3.3.3 Wave parameters and spectrum

In each experiment, the wave spectrum was determined at six locations in the basin (see Fig.3). Three wave height meters (WHM) were placed in the zone without current. Two WHMs were placed in the channel, one on the carriage. The output of the wave height meter on the carriage was used to represent the wave conditions at the measuring section, while the other wave height meters were used to check the uniformity of the wave height in the basin. The information of the wave height meters was all recorded in the computer. With the use of a computer program, it was possible to compute several wave and spectrum parameters. The parameters given by the program were a.o.:

- peak frequency (fp)
- peak period (Tp = 1/fp)
- moments (m0, m2, m4)
- zero crossing period (Tz = (m0/m2)^0.5)
- significant wave height (Hm0 = 4*(m0)^0.5)
- narrowness (ε2)
- broadness factor (ε4)

The program also gave an exceedance curve and an energy density spectrum (see Fig.7). The wave height distribution can be described by a Rayleigh distribution because the spectrum is single topped (Battjes, 1982).

3.3.4 Time- and bed averaging

Local and instantaneous concentration measurements show random variations of 50 to 100% (Bosman, 1982, 1985), because of their sensitivity for local conditions, especially in the near bed zone. A time- and bed-averaging method can be used to reduce variations in the concentration measurements. As in former studies the measuring instruments were mounted on a moving carriage, to perform bed-averaging. This bed-averaging was done perpendicular to the current direction. The carriage moved along the measuring section (length = 0.65 m) vice versa, with a speed of 0.02 m/s (see photo 3).

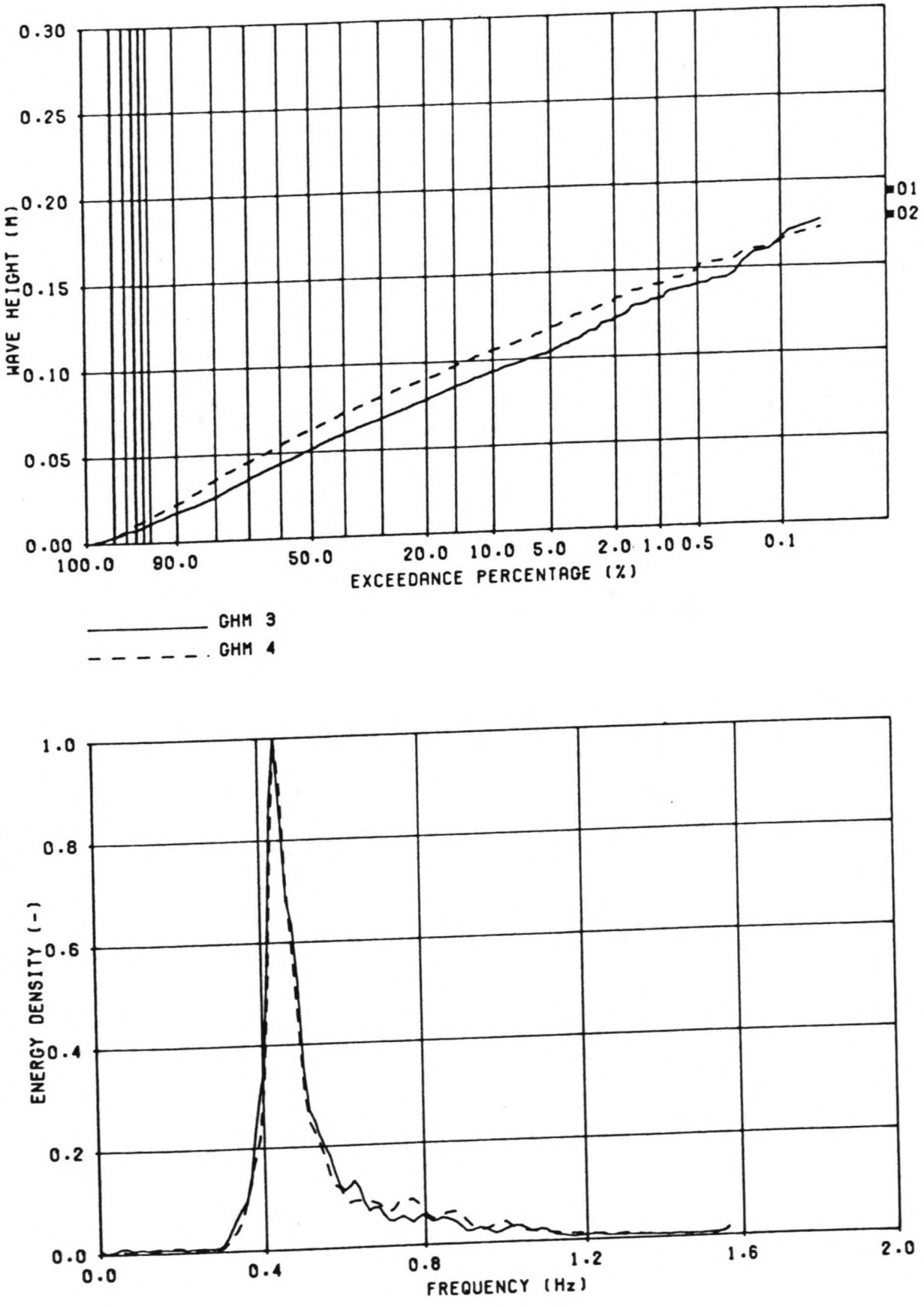

Figure 7 Exceedance curves and energy density spectra (T 10 30 120)

3.3.5 Sediment concentration measurements

The sediment concentrations were carried out using an array of 10 brass intake tubes of 3 mm internal diameter (photo 4). This concentration sampler instrument was attached to the moving carriage; the openings of the intake tubes were placed in current direction. Each tube was connected to a pump, bringing the sediment and water mixture with a 1.5 m/s intake velocity in a 10 l bucket. Ten intake tubes were used to determine the concentration distribution over the water depth (photo 6).

In the earlier 100-mu-study a test was carried out to study the influence of the measuring equipment on the measured concentrations. A comparison was made between the array of 10 intake tubes and a single intake tube. The conclusion was, that the differences in concentration between the array of 10 intake tubes and the single tube are within the standard deviation of the concentrations.

The sediment concentrations were measured by the following procedure, which is almost the same as in the earlier 100-mu-study. First, with the use of the profo, the mean bed level δ was measured. The concentration sampler was then adjusted just above the heighest ripple top. In most cases this was about 1.5 cm above the mean bed level. For adjusting, the reading scale of the sampler was used. This scale was related to the reference level.
The test was now ready to start, the carriage moving and the pumps running for 15 minutes. In this time the ten buckets were filled. After filling, the water in the buckets was poured off and the remaining sediment was washed out in a volume meter (see photo 5). The volume meter consists of 10 small calibrated glass cylinders with decreasing diameters. By reading the height of the sediment in the cylinder, the wet sediment volume was measured. Using a calibration table for each cylinder, the dry mass was determined for every bucket. In the calibration table a correction factor, the so called trapping ratio, was used to determine the concentration properly. This trapping ratio is necessary, because of the fact that the sediment particles cannot completely follow the curved water particles trajectories to the intake tubes (Bosman, van der Velden and Hulsbergen, 1987).
After determining the concentration, again the mean bed level was measured. During each experiment, this procedure was repeated two times. Based on this, a mean, minimum and maximum of the concentrations was determined (see

part F). After the sediment volume measurement, the sediment samples were collected in one sample bottle for analysis of the fall velocities (Wss10, Wss,50, Wss,90) and the particle diameters (Ds,10, Ds,50, Ds,90) of the suspended sediment for each test. These parameters were determined by the Visual Accumalation Tube of Delft Hydraulics.
In some experiments instantaneous sediment concentrations were measured by means of the ASTM (see 3.3.12.).

3.3.6 Water velocity measurements

The velocities were measured with an Electro-Magnetic Velocity meter (E.M.S.), see photo 4. This instrument generates an electro-magnetic field, the degree of disturbance of this field is a measure for the water velocity at the position of the measuring volume of the probe, which is 5 mm below the probe. The time-averaged velocity was determined using a mean value meter (M.V.M). It can average the electronical input signal over a chosen time period. For these measurements a period of 300 seconds appeared to give reproducible results.
The E.M.S was also attached to the moving carriage. The velocities were measured at the same height positions above mean bed level as the intake tubes of the concentration sampler.
For experiments with $\phi=90°$ the E.M.S. measurements were repeated two times, so during one velocity measurement, one concentration test was carried out. Because of the reproducible results in these tests, it was possible to change the procedure for $\phi=60°$ and $\phi=120°$. Now only one velocity measurement was carried out. During this test it was possible to measure the concentration three times. In some tests, instantaneous water velocities were also measured by means of the A.S.T.M. (see section 3.3.12).

3.3.7 Ripple parameters

In each experiment ripple regristations were made using the profo and a penrecorder. These regristations were done before and after every test, in both current and wave direction. For $\phi=90°$ ripple parameters (only in wave direction), were also determined when mean bed level was measured (see 3.3.1).

From these regristrations the following ripple parameters were determined:

- mean ripple height current direction rc
- mean ripple length ,, ,, λc
- mean ripple height wave direction rw
- mean ripple length ,, ,, λw
- parameters (λ1/λ2)c and (λ1/λ2)w, to get impression of the bed regime.

in which:
λ1 = mean upstream length of the ripple.
λ2 = mean downstream length of the ripple.

For ripples in wave direction, these parameters are defined in the same way (see Fig. 8).

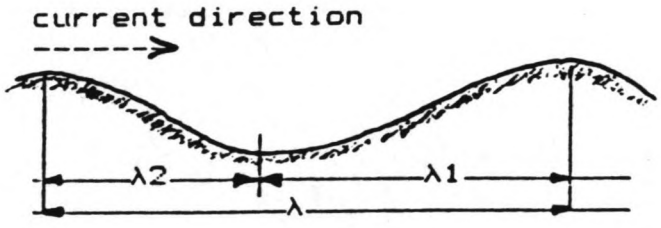

Fig. 8 Upstream and downstream ripple length

3.3.8 Particle diameters of bed material

In each experiment a sample of the bed material at the measuring section was taken with the use of a small grab sampler. After drying the samples, a 30 gr representative part of it was sieved, and the particle size distribution was determined. From this the particle diameters D10, D50 and D90 were computed.

3.3.9 Fall velocity

The suspended sediment samples of each experiment, were analysed in the Visual Accumulation Tube of Delft Hydraulics. In this tube it is possible to determine the particle diameters Ds,10, Ds,50 and Ds,90, and the fall velocity parameters Wss,10, Wss,50, Wss,90. A detailed description of the V.A.T. is given in the 200-mu-study. (Nieuwjaar, van der Kaaij, 1987).

3.3.10 Measuring procedure

A list of the activities, step by step, in the measuring procedure is given here:

Preparation

1. Calibration of the velocity meter (E.M.S.) at still water.
2. Generation of the desired discharge by starting the pumpsystem, and opening the valves.
3. Generation of the desired water depth by the overflow weir.
4. Calibration of the wave height meters.
5. Switching on wave generator.
6. Wait period of at least half an hour for generation of the characteristic ripple pattern.
7. Checking of significant wave height and water depth.

Test measurements

8. Regristration of ripple pattern in wave and current direction, and determination of the mean bed level.
9. Installation of the concentration sampler and the velocity meter at about 1.5 cm above the mean bed level.
10. Starting computer program for data processing of wave height meters, E.M.S. and A.S.T.M.
11. Start pumping out water-sediment samples at 10 heights above mean bed level.(15 minutes)
12. Measuring of fluid velocities at 10 heights above mean bed level.(5 minutes per height)
13. Determination of sediment concentrations with the volume meter and put the samples in the sample bottles.
14. Determination of water depth with gauging stations (see 7.)
15. Regristration of ripple pattern in wave and current direction, and determination of the mean bed level.
16. Reading of wave spectra and wave parameters by running spectrum analyser program, stop data processing.

Points 7 to 16 have been carried out three times for each experiment.

Current alone measurement

17. Switching off wave generator.
18. Determining waterdepth and mean bed level.
19. Measuring of fluid velocity at the measuring section at 10 heights above the bed. (10*5 min.)

At last

20. Turning off the flow by putting off the pump system and closing the valves.
21. Closing the overflow weir.
22. Take a sediment sample at the measuring section.
23. Determining of the particle diameters (Ds,10, Ds,50, Ds,90) and fall velocities (Wss,10, Wss,50, Wss,90) in the accumulation tube (V.A.T.).(This has been done after the experiments were carried out.)

3.3.11 Experimental program.

In the present study, it was not possible to create an experimental program that was quite the same as in the earlier 100-mu and 200-mu studies. This, because of the fact that the maximum water depth in this model was 0.4 m. For this water depth, the maximum significant wave height was approximately 0.14 m. For the mean velocity, Um, the following values were generated:

one pump on : Um = 0.12 m/s
two pumps on : Um = 0.24 m/s
three pumps on : Um = 0.30 m/s

For studying the influence of the current-wave angle on the sediment transport, it was possible to create $\phi=60°$ and $\phi=120°$.
Table 4 gives the experiments carried out in the present study:

For ϕ = 90°

Hsig [m]→ ↓ Um [m/s]	0	0.07	0.10	0.14
0		T 7 0-90	T 10 0-90	T 14 0-90
0.12		T 7 10-90	T 10 10-90	T 14 10-90
0.24		T 7 20-90	T 10 20-90	T 14 20-90
0.30	T 0 30	T 7 30-90	T 10 30-90	T 14 30-90

For ϕ = 60°

Hsig [m]→ ↓ Um [m/s]	0	0.07	0.10	0.14
0				
0.12		T 7 10-60	T 10 10-60	T 14 10-60
0.24		T 7 20-60	T 10 20-60	T 14 20-60
0.30		T 7 30-60	T 10 30-60	T 14 30-60

For ϕ = 120°

Hsig [m]→ ↓ Um [m/s]	0	0.07	0.10	0.14
0				
0.12			T 10 10-120	T 14 10-120
0.24		T 7 20-120	T 10 20-120	T 14 20-120
0.30			T 10 30-120	T 14 30-120

Table 4 The experimental program

The 29 experiments are identified by a test number, given in Table 4. For example; T 7 30-60 stands for an experiment with an approximate significant wave height of 7 cm, and a approximate mean current of 30 cm/s. The current-wave angle here is 60 degrees. The precise values of Hsig and Um are given in the tables.(see part F).

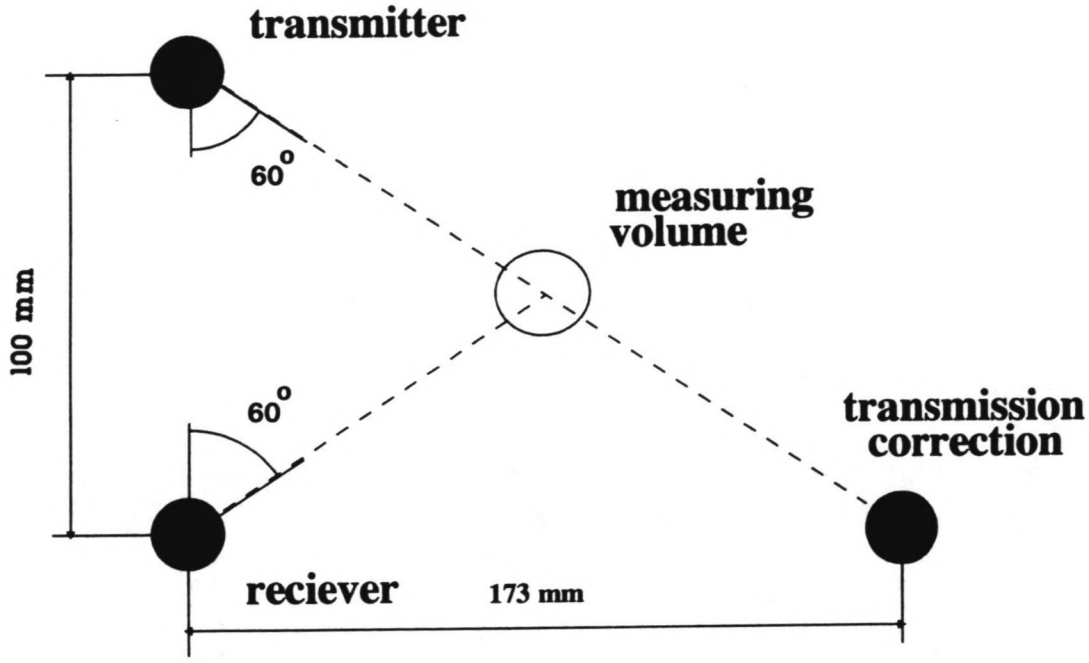

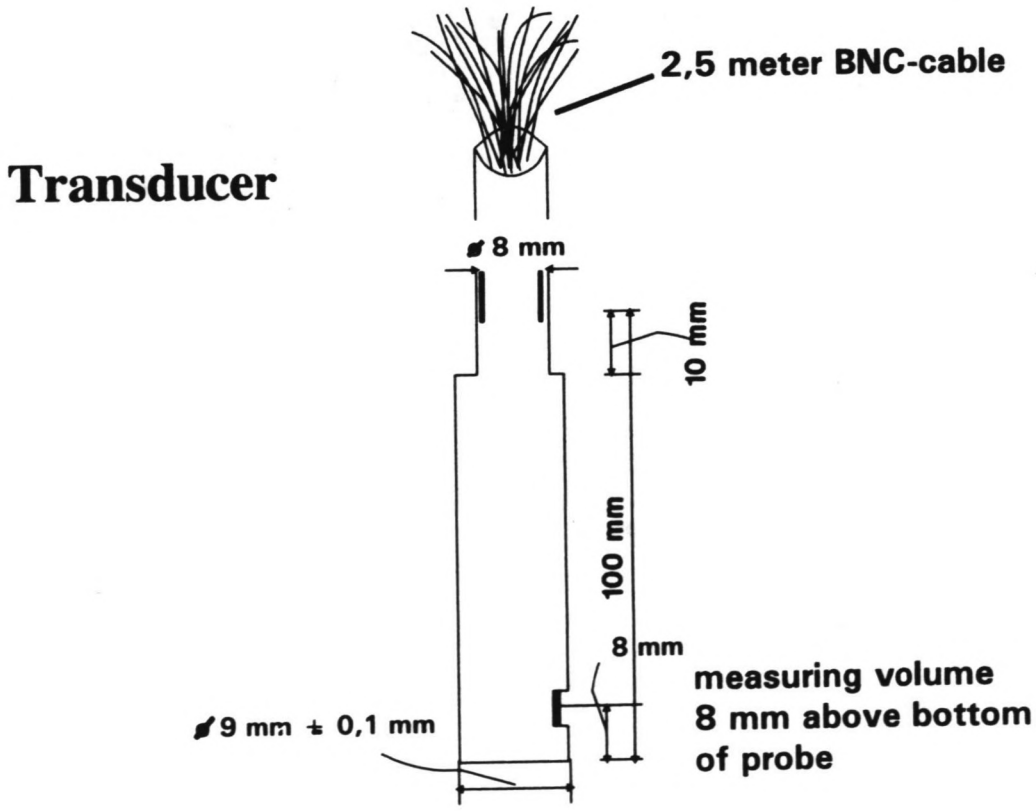

Figure 9 Configuration of ASTM

In some of the experiments also the ASTM was used for measuring both concentrations and velocities.(see next section).
In one experiment (T 10 20-90) the migration of a trench was measured. To get an insight in this migration, the concentrations and velocities were measured at several locations in the trench, at different times. The results are given in section 4.9.

3.3.12 ASTM measurements

Description

During some experiments the instantaneous concentrations and velocities were measured by means of the Acoustical Sediment Transport Meter (ASTM, see photo 4). This instrument determines these parameters by measuring scattered ultrasonic energy. This energy is transmitted by a probe, containing piezoelectric crystals. A transducer recieves the scattered signal from the transmitter. For large sediment concentrations, the received signal is too weak for accurate measurements. Therefore a third transducent acts as a second receiver, and receives directly a part of the transmitted signal.(see Fig.9).

Use of ASTM

The ASTM was used in several experiments. These measurements were always executed in combination with the EMS. During each measurement the measuring time was ten minutes, approximateley the same time as was used for the concentration sampler. Using linear regression on the output signal of the ASTM and the concentrations measured simultaneously with the pump sampler, a calibration factor was computed. This factor had a value of 2.3 for these experiments. The instantaneous concentrations and velocities (recorded by the computer) will be used to estimate the wave-related part of the suspended sediment transport (see also chapter 2). In combination with the EMS (measures velocity in two directions) it is also possible to compute the **cross- shore** sediment transport. The results of these computations will be presented in a later report.

The time-averaged concentrations and velocities (obtained from mean value meters) are presented in the experimental dataset, see part F.

4. Experimental results

4.1 General

In this chapter the results of the experiments are analysed and presented. The present results are compared with the results of the earlier flume study using the same sand material (100μm) (Nap and Van Kampen,1988). This study will herein be referred to as "the earlier 100-mu-study".
In part F of this report the basic data are given in tables. From these, the following parameters have been computed.

- Depth averaged fluid velocity
- The mean sediment loads (three methods)
- The mean sediment transport rates (three methods)

In the present study mean, maximum and minimum values of the measurements are presented.

In the next sections, the following parameters will be described and discussed successively:

- Wave characteristics (4.2)
- Sediment concentration (4.3)
- Fluid velocities (4.4)
- Sediment loads (4.5)
- Sediment transport rates (4.6)
- Ripple parameters (4.7)
- Size and fall velocity of suspended sediment (4.8)

In Section 4.9 the experimental set up of the measurements of the migration of a trench will be described.

4.2 Wave characteristics

4.2.1 Wave spectra

The computed wave spectra are influenced by the current-wave angle. Spectra, measured for $\phi = 60°$, are less narrow than spectra measured for $\phi = 120°$. Similar results were found in the earlier 100-mu-study. In those experiments the difference in narrowness was much more clear because of the fact that the tests were carried out for waves travelling with the current ($\phi = 0°$) and waves travelling against the current ($\phi = 180°$). The broadness factor $\varepsilon 4$ didn´t vary much in the present study.
The averaged values of $\varepsilon 4$ for different ϕ :

$\phi = 90°$: $\varepsilon 4 = 0.536$

$\phi = 60°$: $\varepsilon 4 = 0.560$

$\phi = 120°$: $\varepsilon 4 = 0.522$

So the variations are less than 10%.
An example of a relative narrow spectrum ($\varepsilon 4 = 0.470$ for WHM 4) is given in Fig. 7.

4.2.2 Wave length and peak period

When a current is combined with the waves, the length of the waves will be influenced. For $\phi = 60°$ the wave length will be larger, for $\phi = 120°$ the waves will have a smaller wave length, compared to the situation without a current. This can also be understood from the characteristic wave parameters.
To compute the characteristic wave length, L, and the relative peak period, Tp,rel, the following equations are given (Jonsson et al, 1970):

$$L = cr * Tp \qquad (4.1)$$

$$L' = cr * Tp,rel \qquad (4.2)$$

$$ca = cr + Um \qquad (4.3)$$

$$cr = \sqrt{\frac{g * L}{2 * \pi} * \tanh(2*\pi*h/L)} \qquad (4.4)$$

with:

L	=	wave length without current	[m]
L´	=	wave length in the presence of the current	[m]
Tp	=	absolute wave spectrum period (without current)	[s]
Tp,rel	=	wave spectrum peak period relative to current	[s]
Um	=	depth-averaged fluid velocity	[m/s]
ca	=	absolute wave celerity	[m/s]
cr	=	relative wave celerity	[m/s]
h	=	water depth	[m]
x	=	coordinate in current direction	[m]
y	=	coordinate perpendicular to current direction	[m]

For an extreme situation (most influence on Tp,rel and L) in the present tests, with $\phi = 60°$ and Um = 0.3 m/s the influence on Tp and L is as follows:

cr = 1.88 m/s

Um = 0.3 m/s ---> Um,w = Um * sin 30°
= 0.3 * 0.5 = 0.15 m/s

ca,w = 1.88 + 0.15 = 2.03 m/s

$\phi' = \arctan (ca,x / ca,y)$

ca,x = cr * sin 30° + Um = 1.88 * 0.5 + 0.3 = 1.24 m/s
ca,y = cr * cos 30° = 1.88 * 0.5 * $\sqrt{3}$ = 1.63 m/s

$\phi' = \arctan (1.63 / 1.24) = 53°$

----> Tp,rel = 2.03/1.88 * Tp = 1.08 Tp

----> L = 1.88 * Tp

----> L´ = 1.88 * Tp,rel = 1.08 L

The relative period Tp,rel and the wave length in the presence of the current are only 10% (maximum for these tests) larger than the absolute wave period and the wave length without the current.

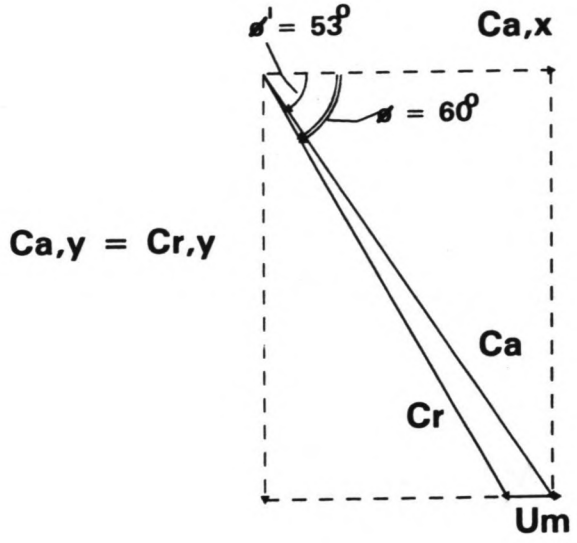

Fig.10 Influence of current strength on wave celerity.

4.2.3 Orbital movement parameters

Two parameters, which characterize the wave action just above the bed, are introduced here:

. Ub = a characteristic orbital horizontal velocity amplitude just outside the wave boundary layer [m/s]

. Ab = a characteristic orbital horizontal displacement amplitude just outside the wave boundary layer [m]

These parameters are computed using the significant wave height Hsig as characteristic wave height. The characteristic wave length, L, and the relative wave spectrum peak period, Tp,rel, as computed in the following formula, to account for the presence of the current:

$$Ub = \frac{\pi * Hsig}{Tp,rel * \sinh(2*\pi*h/L)} \qquad (4.5)$$

$$Ab = \frac{Hsig}{2 * \sinh(2*\pi*h/L)} \qquad (4.6)$$

The results of the above computations are given in Table 4.1.

4.3 Sediment concentrations

4.3.1 General

The measured time- and bed averaged concentration profiles for all experiments are presented in Figs. 4.1 - 4.3 (part F), in which the mean concentration values at different heights above mean bed level. The concentration values are also given in the experimental data tables (part F). As in the earlier 100-mu-study, the time- and bed-averaged concentration profile for each experiment was determined as follows:

1) For each intake tube, the heights above mean bed level were averaged over all three tests.
2) The measured concentrations for each intake tube were averaged over three tests.

This method is only allowed, if the height of the mean bed level does not vary too much. For most of the tests this was true indeed, but when larger height variations were found (> 4 mm), the concentration was computed by linear interpolation between the values measured at different heights.

4.3.2 Wave height influence

The significant wave height, Hsig, influences the concentration profile; the Figs. 4.1.A - E show:

. Increasing the significant wave height, Hsig, leads to an increase of concentrations.

. Increasing the significant wave height, Hsig, does not lead to a steeper concentration profile.

These tendencies were also noted in the earlier 100-mu-study.

4.3.3 Current velocity influence

The current strength influences the concentrations as follows (see Figs. 4.2.A - D)

. Increasing the current strength leads to a more uniform distribution over the depth.

. Increasing the current strength causes an increase in the concentrations in the upper layers.

. The highest concentrations in the near bed zone are obtained in case of waves alone. When superimposing a weak current (0.12 m/s), this leads to a significant lower concentration. Increasing the current (0.24 - 0.30 m/s) leads to a small increase of the concentration in the near bed zone.

These conclusions were also given in the earlier 100-mu-study, although the phenomenon described in the third conclusion seems to be present more clearly in the experiments of the present study.

4.3.4 Current direction influence

The current-wave angle, ϕ, influences the concentration profile as follows (see Figs. 4.3.A - E):

. The experiments for $\phi = 90°$ generally give the highest concentrations, especially for increasing wave heights.

. There is no clear difference in the concentration profile for $\phi = 60°$ and $\phi = 120°$.

The reason for this may be that for $\phi = 90°$ a "honeycomb-ripple pattern" is created. This pattern induces more turbulence because of the fact that it is "more" 3-dimensional than the ripple pattern that is created by the other current-wave angles.

4.4 Fluid velocities

4.4.1 General

The time- and bed-averaged velocities were measured as described in Section 3.3.6.
For $\phi = 90°$, three velocity profiles were measured (and averaged), for the other angles this was done only one time. For comparison of the velocity profiles, measured in different experiments, the measured velocities and the heights above the mean bed level have been made dimensionless (see Figs. 4.4 - 4.5). The time- and bed- averaged velocities U(z) are divided by the depth-averaged velocity, Um. The mean heights above the mean bed level, z, are divided by the mean water depth, h.

To determine the depth-averaged velocity, Um, from the measured velocities, two assumptions have been made (see Fig. 11)

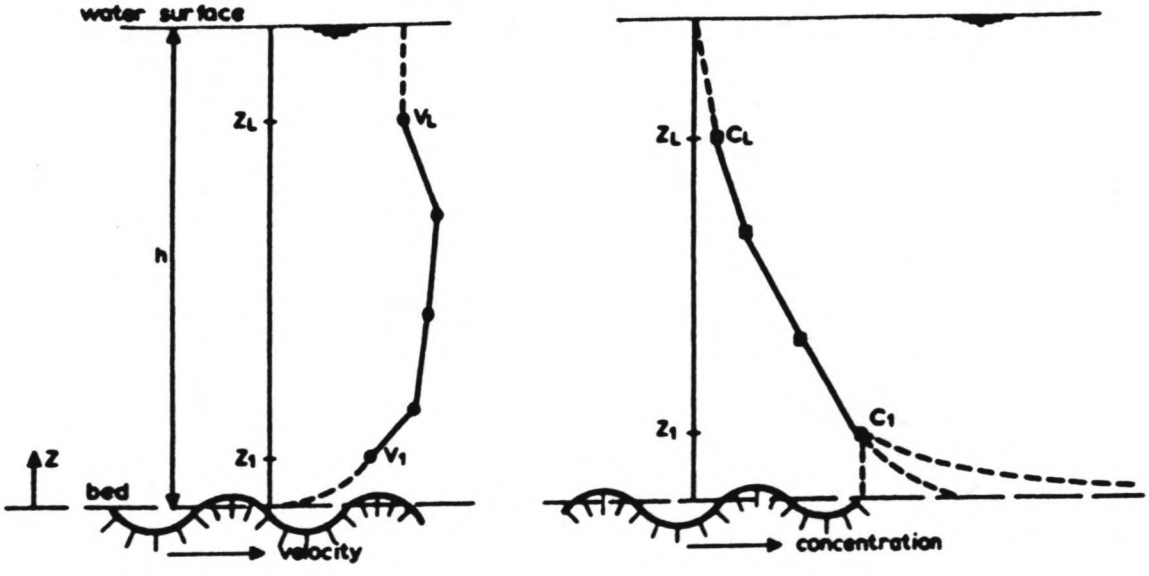

Fig. 11 Extrapolation of velocity and concentration profiles

1. The velocities between the mean bed level and the lowest measuring point are represented by a function, corresponding with a logarithmic velocity distribution in case of a rough bed (Van Rijn,1986):

$$U(z) = U1 * (z/z1)^{0.25} \quad \text{, for } 0 < z < z1 \qquad (4.7)$$

in which :

U1 = fluid velocity in first meas. point above the bed [m/s]
z1 = height above bed of first measuring point [m]
z = height above mean bed level [m]

2. The mean velocity between the highest measuring (z10) and the water surface are assumed to be equal to the measured velocity (u10) in the highest measuring point.

Now, the depth-averaged fluid velocity is determined as :

$$Um = 1/h \sum_{i=1}^{N} (Ui + Ui-1) * (zi - zi-1) / 2 \qquad (4.8)$$

with:
Um = depth averaged fluid velocity [m/s]
Ui = mean time- and bed-averaged velocity at height zi above mean bed level [m/s]
N = total number of points (including extra polated points) [-]
h = water depth [m]

4.4.2 Current alone

In each experiment current velocities were also measured in the absence of waves. This was done to determine the bed roughness, caused by the bed forms, generated by waves and a current. During three current alone experiments (T (7) 0 30, T (10) 0 30 and T (14) 0 30) sediment transport rates were also measured. These experiments were done after respectively the experiments: T 7 30-90, T 10 30-90 and T 14 30-90. This was done, to get an impression of the influence of the bed forms on the sediment transport (see

also Table 4.2). Current alone experiments for weaker currents were not usefull in this respect because of the fact that little sediment was brought in suspension then.

In this section the velocity profile, in case of current alone will be analysed. This was done by comparison of the measured velocity profile, with a theoretical logarithmic distribution, presented as:

$$U(z) = (U*/\kappa) * \ln (z/z0) \qquad (4.9)$$

with:

U(z)	= current velocity at level z	[m/s]
U*	= bed-shear velocity	[m/s]
z	= height above mean bed level	[m]
z0	= roughness length scale (zero-velocity level)	[m]
κ	= the von Karman constant (=0.4)	[-]

The bed roughness length of Nikuradse, Ks, is computed as:

$$Ks = 33 * z0 \qquad (4.10)$$

In contrast with the earlier studies, in the present study there was only little influence of side wall effects. It was possible now to use all the ten measuring points in the fitting procedure. The regression factor was always higher than 0.98. The examination of the bed roughness related to ripple parameters will be discussed in Chapter 5.

4.4.3 Wave influence

The velocity profiles measured in the presence of waves are shown in Figs.4.4.A - 4.5.E.

As can be observed in these figures, the measured velocity profiles differ for varying wave heights and current-wave angles:

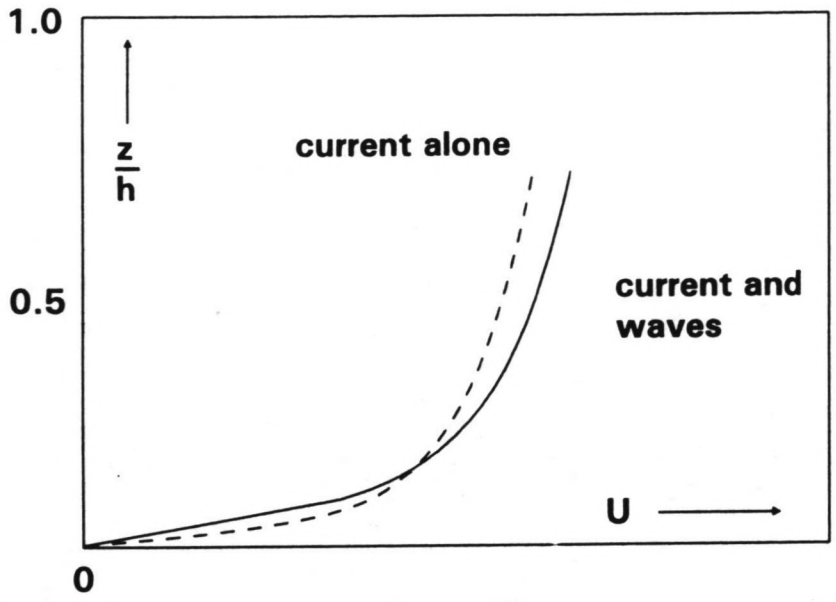

Figure 12A Velocity profiles for current and waves and current alone

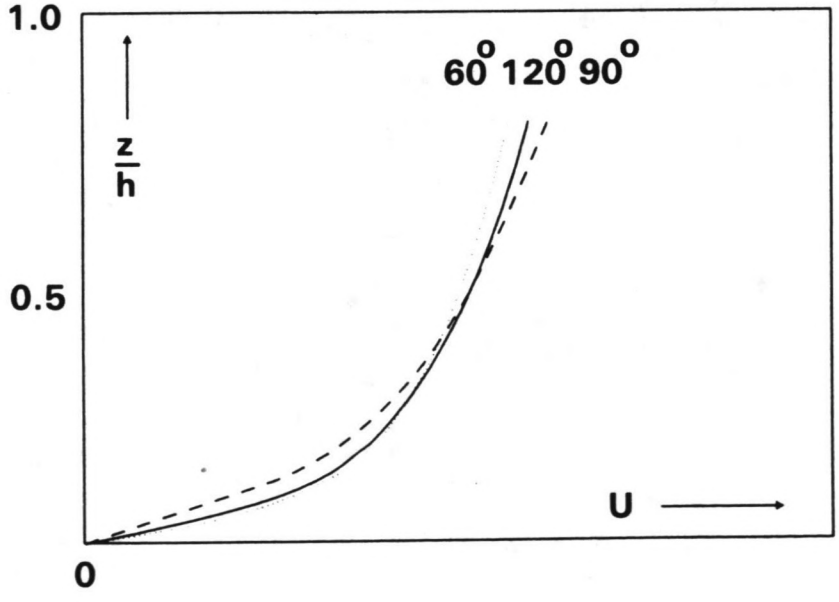

Figure 12B Velocity profiles for different current-wave angles

Influence wave height:
Compared with current velocities when waves are absent, the velocities measured for current and waves are (see Fig. 12.A):

- Relatively small in the near bed zone ($z/h < 0.25$)
- Almost equal in the middle layers ($0.25 < z/h < 0.5$)
- Relatively large in the upper layers ($z/h > 0.5$)
  - . Increasing the current strength, Um, at a constant wave height, leads to a decrease of the differences.
  - . Increasing the significant wave height, Hsig, at a constant current velocity, leads to an increase of the differences.

The differences are largest in case of a large wave height in combination with a weak current.

Influence current-wave angle:
The influence of the angle between wave direction and current direction can be observed from Figures 4.4.A - E. The general trend is presented in Fig. 12.B.

. The velocities in the near bed zone are relatively small for $\phi = 90°$ and relatively large for $\phi = 60°$.
. In the middle layers, no real differences are found.
. The velocities in the upper layers are relatively large for $\phi = 90°$ and relatively small for $\phi = 60°$.(see Fig. 12.B)

In the earlier 100-mu-study it was found that the velocities in the near bed zone were relatively small for opposing waves ($\phi = 180°$) compared to following waves. This tendency was also found in the present study, although the differences were considerably smaller, which is logic because $\phi = 120°$ is a smaller angle than $\phi = 180°$. In the upper layers the velocities are relatively large for opposing waves (found in both studies).
Striking is that the velocities in the near bed zone have the lowest values for $\phi = 90°$. The cause of these differences is related to the (complicated) interaction between the waves and the current and the generated ripple patterns.

4.5 Sediment loads

4.5.1 General

The sediment load is defined as the total amount of moving sediment per unit bed surface area:

$$Lt = \int_{z=0}^{h} c(z)\, dz \qquad (4.11)$$

with:

Lt	= total Load	[kg/m²]
c(z)	= time- and bed-averaged concentration at z	[kg/m³]
h	= water depth	[m]

Here, the total load consists of two parts, the bed load and the suspended load:

$$Lb = \int_{z=0}^{r/2} c(z)\, dz \qquad (4.12)$$

$$Ls = \int_{z=r/2}^{h} c(z)\, dz \qquad (4.13)$$

$$Lt = Lb + Ls \qquad (4.14)$$

with:

Lb	= bed load	[kg/m²]
Ls	= suspended load	[kg/m²]
r	= mean ripple height	[m]

In the present study, only the suspended load was computed. Comparison with former study is possible because, as was concluded in the earlier 100-mu-study, the influence of the bed load transport on the total transport is small (Sb/St*100% < 7%).

4.5.2 Extrapolation of concentrations in unmeasured zones

To compute the sediment load, the concentrations in the zones below the lowest and above the highest measuring point must be known. This was done by extrapolation. Three extrapolation methods were used:

method 1

The sediment concentrations between the bed (z = 0 m) and the first measuring point (z = z1) are assumed to be equal to the concentration (c1) in the first measuring point (see Fig. 11). Thus:

$$c = c1 \qquad \text{for } 0 < z < z1 \tag{4.15}$$

This method is supposed to give an under limit.

method 2

The sediment concentrations between the bed (z = 0.001 m) and the first measuring point are computed by (see Fig. 13):

$$c = A\,Y^{B} \qquad \text{for } 0.001 < z < z1 \tag{4.16}$$

in which:

Y = (h-z)/z = dimensionless vertical coordinate
z = vertical coordinate above bed
h = water depth
A,B = coefficients

The A and B coefficients are determined by a regression method applying the measured concentrations of the first three measuring points above the bed, as follows:

. select B = 0.1,

$$\text{. compute } A = \sum_{1}^{3} (Yk^{B} * ck) \Big/ \sum_{1}^{3} (Yk^{B}\, Yk^{B}), \tag{4.17a}$$

$$\text{. compute } T = \sum_{1}^{3} (A\, Yk^{B} - ck), \tag{4.17b}$$

. select B = 0.2 (B is varied over the range 0.1 to 5),

. repeat procedure.

Finally, the A and B coefficients corresponding to a minimum T-value are selected as the "best" coefficients. Applying Eq. (4.16), the sediment concentrations are computed in 50 (equidistant) points between the bed (defined at z = 2 * d50) and the first measuring point (z = z1). The maximum concentration is assumed to be 1590 kg/m³.
This method is supposed to give an upper limit.

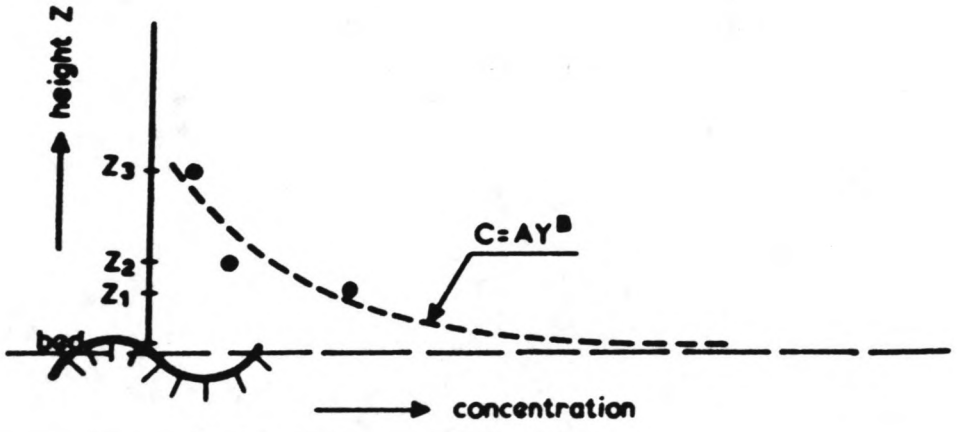

Fig. 13 Regression of concentration profile (method 2)

method 3
The sediment concentrations between the bed and the first measuring point are represented by (Fig. 14)

$$c = e^{Az + B} \quad \text{for } 0 < z < z1 \tag{4.18}$$

in which:
z = height above bed
A, B = coefficients.

The A and B coefficients are determined by a linear regression method applying the measured concentrations of the first three measuring points above the bed, as follows:

$$A = \frac{3 \sum_{1}^{3} (zk \ln ck) - \sum_{1}^{3} (zk) \sum_{1}^{3} (\ln ck)}{3 \sum_{1}^{3} (zk\ zk) - (\sum_{1}^{3} zk)^2} \qquad (4.19)$$

$$B = \frac{\sum_{1}^{3} (zk\ zk) \sum_{1}^{3} (\ln ck) - \sum_{1}^{3} (zk) \sum_{1}^{3} (zk \ln ck)}{3 \sum_{1}^{3} (zk\ zk) - (\sum_{1}^{3} zk)^2} \qquad (4.20)$$

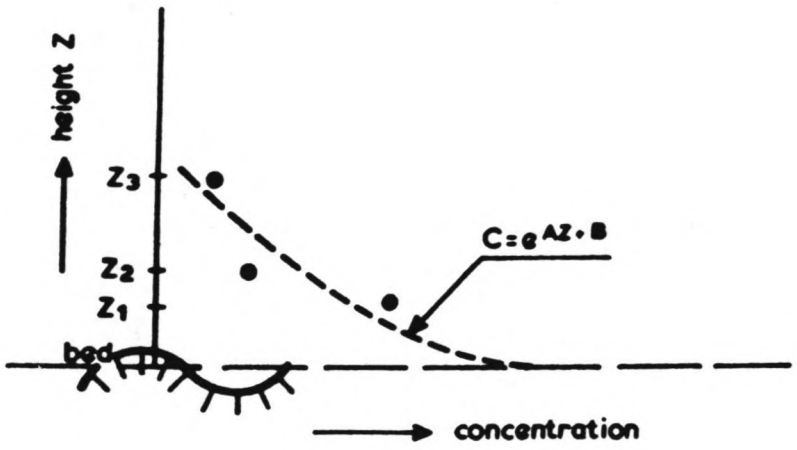

Fig. 14 Regression of concentration profile (method 3)

Applying Eq. (4.18.), the sediment concentration are computed in 50 (equidistant) points between the bed (defined at z = 2*d50) and the first measuring point (z = z1). The maximum concentration is assumed to be 1590 kg/m³.

The applied method for further computation

As described above, three methods were used for computation of the concentrations in the unmeasured zones. The values found for Cbed (defined as the concentration at z = 2*d50 above the bed and determined by extrapolation) are presented in part F. The results, when using the second method, are quite different when compared to method 1 and method 3. This,

because the second method is supposed to give an upper limit. In several experiments this method gives the maximum concentration for Cbed, and therefore significant higher values for the suspended loads and transport rates. On the other hand, method 1 and 3 gave comparable results (mean difference less than 1%). Because of these facts it was decided that method 2 was not applicable for further computation. The values of Ls are the averaged values of method 1 and 3 and are presented in Table 4.2.

4.5.3 Wave height influence

Increasing the wave height Hsig, leads to a larger load. Table 5 shows the wave height influence. For example, an increase of the wave height from Hsig = 0.07 to 0.14 m (at a current velocity Um = 0.12 m/s and a wave-current angle ϕ = 90°) leads to an increase of the total load by a factor 7. A comparison is made between the present study and the earlier 100-mu-study. For the earlier 100-mu-study the values were interpolated.

Um [m/s]	Increase of Total Load by Increase of Hsig from 7 to 14 cm				
	present study				earlier study
	ϕ=90°	ϕ=60°	ϕ=120°	mean	mean
0	9	-	-	9	16
0.12	7	11	-	9	11
0.24	8	4	2	5	7
0.30	4	2	-	3	5

Table 5 Increase factors

From Table 5 it appears that the increase of the suspended load becomes less pronounced with increasing current strength. The increase factors for the present study are somewhat lower than the increase factors given in the earlier 100-mu-study. Striking is the difference in the increase factor for waves alone. The suspended load for waves alone (see part F, Table 4.2) is significantly higher (about 60%) in the present study compared to the earlier 100-mu-study. A clear reason cannot be given for this phenomenon. The difference can only be explained by experimental deviations in particle diameter, wave height, wave period and the possible presency of a "background concentration" for these experiments.

4.5.4 Current strength influence

In Table 6 the influence of the current strength on the suspended load is presented. A same tendency as for the wave height influence is found.

Increase of Total Load by Increase of Um from 0.12 to 0.30 m/s		
Hsig (cm)	present study mean	earlier study mean
7	7	6
10	2	3
14	2	2

Table 6 Increase factors

. A larger significant wave height causes a less pronounced increase of loads with increasing current strength.

From Table 6, it is clear that the differences in the increase factors for both studies are minimal. From the Figures 4.6.A - C and Table 4.2. one can observe that:

. A weak current (Um = 0.12 m/s) superimposed on the waves leads to a decrease of the loads. This conclusion was also made in the earlier 100-mu-study, but no reasonable explanation can be given for this phenomenon.

. The wave direction does influence the suspended load in the present study. The suspended load for $\phi = 90°$ was about 50% larger than the suspended load for $\phi = 60°$ and $\phi = 120°$. For those current-wave angles the results were comparable.

. The increase of loads by increasing Hsig or Um in this study don´t differ much from the earlier 100-mu-study. The largest deviations are caused by the relatively large suspended loads in case of waves alone in this study. A clear explanation can´t be given for this yet.

4.6 Sediment transport rates

4.6.1 General

As is pointed out in chapter 2, the sediment transport rates are computed from the time- and bed-averaged concentrations and velocities. In this section only the time- and bed- averaged sediment transport will be discussed, so, the wave- related part of the total sediment transport will be neglected here.
The definition for the suspended sediment transport (Ss) is:

$$Ss = \int_{r/2}^{h} c(z) * u(z)\, dz \qquad (4.21)$$

with :

Ss = suspended sediment transport [kg/ms]
r = mean ripple height [m]
c(z) = Time- and bed-averaged concentration at height z [kg/m³]
u(z) = Time- and bed-averaged fluid velocity at height z [m/s]

4.6.2 Suspended sediment transport

Numerical computations of the depth-integrated suspended sediment transport (Ss) requires the specification of velocities and concentrations at equal elevations above the bed (at equal z-values). When the z-values of the velocities are not correspondending, linear interpolation is applied to obtain the required data.

The depth-integrated suspended sediment transport (Ss) is computed as:

$$Ss = \sum_{i=1}^{n} 1/2\ (Ui * ci + Ui\text{-}1 * ci\text{-}1) * (zi - zi\text{-}1) \qquad (4.22)$$

in which:

Ui = fluid velocity at height zi above the bed [m/s]

ci = sediment concentration at height zi above the bed [kg/m3]

N = total number of points (incl. extra- and interpolated values) [-]

Three different methods (see Section 4.5.2) are applied to represent the sediment concentrations in the unmeasured zone near the bed, so three different values of the suspended sediment transport are obtained and implemented in the data base (Ss1, Ss2, Ss3). The results are given in the data tables of part F. The average value of Ss1 and Ss3 is used as the suspended load transport (see Table 4.2 and Section 4.5.2.)

4.6.3 Relationship between Ss, Hsig and Um and ϕ

In Section 4.6.2 the computation has been explained. Now it is possible to study the relationship between the suspended sediment transport and the parameters Hsig and Um. These values are presented in Table 4.1. This relationship is presented in Figs. 4.7.A - B.

It is clear that increasing Hsig and Um will increase the suspended sediment transport.

1. Influence wave height

The relation between Ss and Hsig will be investigated. This relation can be described by (for Um = constant):

$$Ss \approx Hsig^{q} \qquad (4.23)$$

In which q still depends on the depth-averaged fluid velocity, Um and also (as is shown below) on the current-wave angle, ϕ. The parameter q is computed for constant Um and ϕ, by linear regression of varying significant wave heights.(In fact the suspended transport is better described by: $Ss = \alpha (H_{sig})^{q}$ and $Ss = \beta (U_m)^{y}$, however in the present study it appeared that $\alpha \approx \beta \approx 1$.)

The results are presented in Table 7:

Um [m/s]	mean q	ϕ = 90 q	ϕ = 60 q	ϕ = 120 q
0.12	2.4	2.3	2.5	2.4
0.24	1.8	1.8	1.8	1.8
0.30	1.4	1.3	1.4	1.6

Table 7 Dependence of Ss on Hsig

It is noticable that q has higher values for $\phi = 60°$ and $\phi = 120°$ than for $\phi = 90°$. The conclusion is that the suspended sediment transport rate is somewhat lower for those angles. When the q values are compared with the values found in the earlier 100-mu-study ($\phi = 0°$ and $\phi = 180°$), it appears that the lowest values are found for $\phi = 90°$, and then increasing for smaller angles. (90 - 60 - 0 or 90 - 120 -180)

2. Influence velocity

The relationship between the suspended sediment transport and the depth-averaged velocity will be investigated. The relation is presented by:

$$Ss \approx Um^{y} \qquad (4.24)$$

In which the parameter y still depends on the significant wave height. Again by linear regression Table 8 gives the values of y for different Hsig and ϕ.

H_{sig} [m/s]	mean y	ϕ = 90 y	ϕ = 60 y	ϕ = 120 y
7.0	3.3	3.2	3.4	3.2
10.0	2.8	2.7	2.9	2.7
13.5	2.4	2.2	2.5	2.6

Table 8 Dependence of Ss on Um

The increase of Hsig leads to a decrease of y, meaning a less pronounced increase in suspended transport with increasing Hsig. When compared to the earlier 100-mu-study, y has the lowest value for $\phi = 90°$ and higher values for decreasing angles, but this tendency is not as obvious as found for q. The differences in y are smaller for varying angles.(Fig. 4.7.B)

Conclusions influence Hs and Um on Ss

From the analysis under 1. and 2. the following conclusions can be drawn:

- In this study the parameter q is significant lower than in the earlier 100-mu-study, and the parameter y differs not much when compared to the earlier 100-mu-study (under same conditions). From the computations one can conclude that the suspended sediment transport is relatively large for $\phi = 90°$.

- The values of q and y are decreasing for increasing Um and Hsig. This means a less pronounced increase of the suspended sediment transport with increasing Um, Hsig.

3. Influence of current-wave angle

The influence of the angle ϕ (between the wave and current direction) on the sediment transport is studied. The results of the earlier 100-mu-study have also been taken in consideration.

To make a fair comparison for all experiments, (water depth in present study is 0.4 m, and 0.5 m in earlier study) it is necessary that the sediment transport rates are compared under same (wave and current) conditions. The values of Ss in the experiments of the earlier 100-mu-study and the present study have been standarised for values of Ub (0.15, 0.20, 0.30 m/s) and Um (0.12, 0.24, 0.30). See Table 4.6. This was done by estimating Ss with the Tables 7 and 8, for the mentioned values of Hsig and Um.

Example estimating Ss*

As an example of this calculation, the value of Ss* (standarised value of sediment transport rate) will be computed for experiment T10 20-120.

T10 20-120:

Smeas = 19.50 g/m.s

Hsig1 = 11.3 cm --> Ub1 = 24.3 cm/s
Um1 = 24.65 cm/s (see Table 4.1, measured values)

According to Table 7: $Ss=(H_{sig})^{1.8}=(0.113)^{1.8}$= 19.75 g/m.s

According to Table 8: $Ss=(U_m)^{2.7}=(0.2465)^{2.7}$= 22.80 g/m.s

As estimation for Ss the average value is computed:

Ss1 = (19.75 + 22.80)/2 = 21.28 g/m.s

(Ss1 is the estimation of Ss from the measured wave- and current parameters.)

For the standard values the estimations are:

Ub2 = 20 cm/s --> Hsig2 = (20/24.3)*Hsig1 = 9.3 cm

Ss = $(0.093)^{1.8}$ = 13.91 g/m.s (see Table 7)
Ss = $(0.24)^{2.7}$ = 21.21 g/m.s (see Table 8)

----> Ss2 = (13.91 + 21.21)/2 = 17.56 g/m.s

(Ss2 is the estimation of Ss from the standarised wave- and current parameters.)

The value of Ss* is now computed as:

Ss* = (17.56/21.28) * 19.50 = 16.09 g/m.s

For this experiment it appears that the values of Hsig (Ub) and Um were higher than the standarised values. Hsig had a value that was 21.5% too large (11.3/9.3 = 1.215) , and Um was 2.7 % (24.65/24 = 1.027) too large.

According to the computation method as described above, based on the Tables 7 and 8, the measured value of Ss should have a value that was 21.2% too large (21.28/17.56 = 1.212). The value of Ss* is then computed as:

Ss* = Smeas/1.212 (for T1020-120)

This method has been applied to all experiments. The values of Ss* are presented in Table 4.6.

Empirical sediment transport formula

It is possible to represent the Ss-values by an empirical sediment transport formula, wherein Ss depends on Um,Ub and ϕ. Although the formula will not be correct, one can get a better insight in the relationship between Ss and Um,Ub,ϕ, and the importance of the several parameters.
For these studies a formula is chosen in the form:

$$Ss = a(\phi) * b * Um^{c} * Ub^{d} \qquad (4.25)$$

case 1

In this case, the influence of ϕ on Ss is neglected ($a(\phi) = 1$). The values found for c,b and d that were computed by linear regression:

----> b = exp(3.107) ≈ 22.4
       c = 2.731
       d = 2.154

For the correlation factor ρ, a value of 0.933 was found. The correlation factor gives an estimation of the reliability of the formula, which is maximal for $\rho = 1.00$.

case 2

The mean values of $a(\phi)$ and its standard deviation s are computed from the measurements:

```
----> a(0)   = 0.7   with s = 0.13  (19%)
      a(60)  = 1.0        s = 0.21  (21%)
      a(90)  = 1.4        s = 0.28  (20%)
      a(120) = 1.1        s = 0.30  (27%)
      a(180) = 0.9        s = 0.16  (18%)
```

See also Table 4.6.
With linear regression the values of b,c and d can be computed. The results were:

```
----> b = exp(2.934) ≈ 18.8
      c = 2.695
      d = 2.073
```

For this computation the correlation between Ss* and the used formula has a value of ρ=0.939

case 3

The factor a(ϕ) is assumed to be dependent on the ratio Ub/Um. For small values of Ub/Um, a(ϕ) should become close to 1.0 for all angles, because of the fact that the influence of ϕ on Ss is small for relatively small wave heights. The relationship that was found assuming linear dependence for varying ϕ:

```
a(0)   = 0.81  -  0.11 Ub/Um
a(60)  = 1.17  -  0.16 Ub/Um
a(90)  = 1.14  +  0.20 Ub/Um
a(120) = 1.01  +  0.06 Ub/Um
a(180) = 0.90  -  0.01 Ub/Um
```

The correlation for this relationship was not very high, so the correlation between Ss* and this empirical formula did not increase. The results computed by linear regression:

```
----> b = exp(2.985) ≈ 19.8
      c = 2.622
      d = 2.162
```

The simplification of using the mean values of a(ϕ) (no dependence on Ub/Um) appears to be allowed for this range of Ub/Um. This formula is applied in the computations (see Figs. 4.7.C - E). In Table 4.7, part F a comparison is made between the measured sediment transport and the used sediment formula.

Influence ϕ on Ss

From the Figs. 4.7.C - E it is clear that the maximum Ss rate is reached for $\phi = 90°$ and the minimum for Ss = 0°, according to the mean a(ϕ)-values. The influence of ϕ can be important, even a factor 2 in these experiments is found when comparing the sediment transport rates for perpendicular waves with following waves.

However, the variations in the a(ϕ) factor are not only related by the current-wave angle, ϕ. The variations may also be related to small differences in the experimental conditions, variations in pump discharge and variations in particle sizes before and after replenishment of the channel bed. When comparing the earlier 100-mu-study to the present study, the side walls of the flume and the guiding plates in the basin can give an extra deviation in the measured sediment transport. Besides, comparing results of two different studies should always be done with care.

Another remark must be made for the mean velocity Um, and its relationship to sediment transport when the transports are compared for different water heights. It is known, that in the earlier 100-mu-study h = 50 cm, and in the present study h = 40 cm. As is described above the standarised sediment transports are computed for same Ub, Um. However, when Um is equal for different water heights, it is not true that the sediment transport is influenced in the same way.

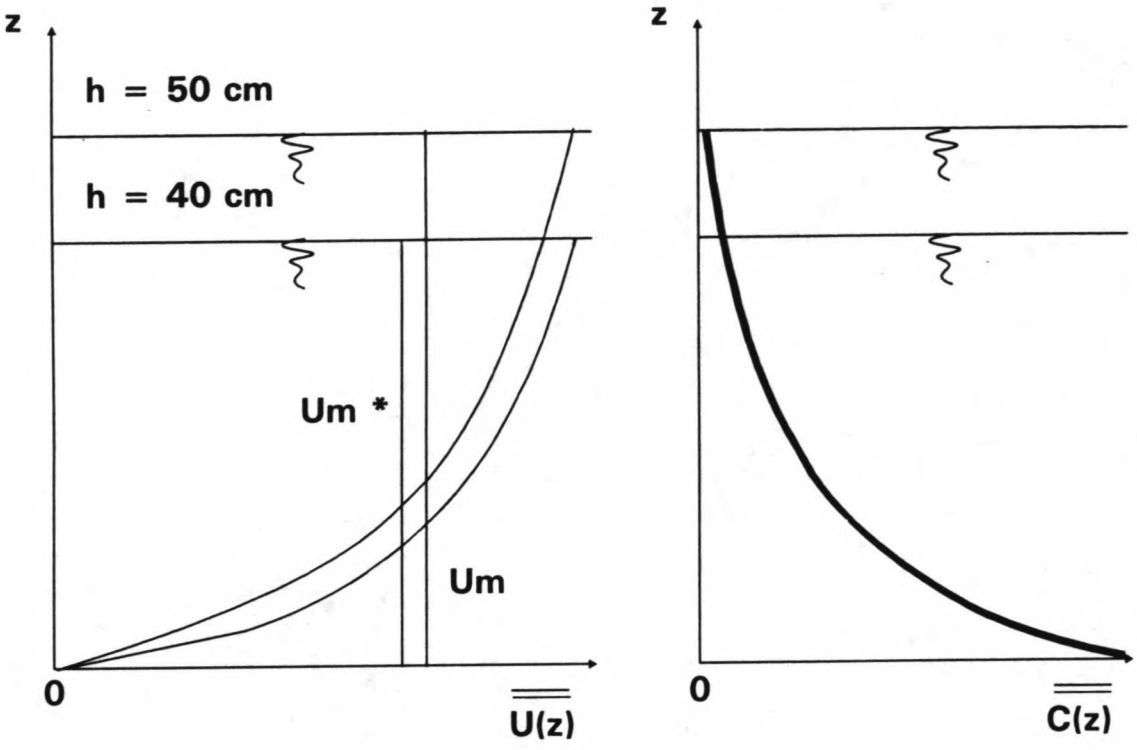

Figure 15 Influence of changed h on Um, and its relationship to Ss

For h = 50 cm, U(z) is relatively small in the near bed zone (where the sediment transport contribution is high), and relatively high in the upper layer (40 cm < z < 50 cm). In the upper layer there is almost no contribution to the sediment transport (see Fig. 15). For the earlier 100-mu-study this was about 2% of the total transport. When this upper layer is taken out of consideration, Um decreases. For $\phi = 0°$ this decrease is 3% (Um* = 0.97*Um) for $\phi=180°$, 7% . The sediment transports that are measured in the earlier 100-mu-study, are found for "smaller" Um-values. This means that the sediment transport rates for that study are larger, according to the empirical formula, 7% for $\phi = 0°$ and 20% for $\phi = 180°$. The $a(\phi)$-factor for $\phi = 0°$ should become more close to 0.8 and for $\phi = 180°$ close to 1.1, but a more detailed computation is usefull. Therefore in the analysis this phenomena is not taken into account.

From the mean $a(\phi)$-values and its standard deviations it is possible to compute the chance that $a(\phi 1) > a(\phi 2)$, in which $\phi 1$, $\phi 2$ are different current-wave angles. This computed chance gives an insight in the

reliability of the results. For every a(ϕ), mean (μ) and standard deviation (s) are known, so this chance can be computed by the Student-distribution. This computed chance gives an insight in the reliability of the results of the experiments. For example, (according the experiments) the chance that the sediment transport for a current-wave angle of $\phi 1 = 90°$ will be larger than the sediment transport for a current-wave angle of $\phi 2 = 0°$, is 99% . When considering two other wave-current angles, for example $\phi 1 = 60°$, $\phi 2 = 120°$, this chance is only 60% , so one can conclude that there is no clear difference in the sediment transport rate for these angles. In Table 9 this chance is presented for all a(ϕ)-factors.

$\phi 1$ \ $\phi 2$	0	60	90	120	180
0	*	0.12	0.01	0.12	0.17
60	0.88	*	0.13	0.40	0.64
90	0.99	0.87	*	0.76	0.94
120	0.88	0.60	0.24	*	0.72
180	0.83	0.36	0.06	0.28	*

Table 9 $P(a(\phi 1) > a(\phi 2))$

From Table 9 one can see that a high reliability is reached for $\phi = 90°$ and $\phi = 0°$. To the author´s opinion one may conclude that in general the maximum sediment transport is obtained for $\phi = 90°$ and the minimum sediment transport is obtained for $\phi = 0°$. For the other angles ($\phi = 60°,120°,180°$) one cannot conclude that there are differences in the a(ϕ)-values. The reliability is too low for making that conclusion. One can only conclude that for those current-wave angles the sediment transport rate should have a value between the sediment transport rates found for $\phi = 0°$ and $\phi = 90°$.

Finally, attention is paid to a remarkable fact. In the Tables 13 and 14 (Chapter 5) the dependence of the apparent roughness increase on the current-wave angle, ϕ, is presented. Striking is the similarity in $\gamma(\phi)$, the ratio Ks,app/Ks,phys and a(ϕ). From these data one can conclude that there is relationship between the apparent roughness increase (expressed in γ) and the suspended sediment transport (expressed in a).
For a current-wave angle of 90° the apparent roughness increase is maximal. The suspended sediment transport is also maximal for that current-wave angle. This phenomena could be explained by the fact that the influence of

the waves perpendicular to the current direction, will influence the flow (velocity distribution) most. The velocities in the near bed zone will decrease (rough bed) and the concentrations will increase in the near bed zone. For the suspended sediment transport this are two opposite effects (higher concentrations, lower velocities).

Conclusions influence ϕ on Ss

Although the correlation ρ doesn't increase much (from 0.933 to 0.939) when the influence of ϕ is taken into account in the sediment transport formula, one can conclude that:

- the current-wave angle ϕ influences the sediment transport rate
- the largest sediment transport rates are obtained for a current-wave angle of $\phi = 90°$.
- the smallest sediment transport rates are obtained for a current-wave angle of $\phi = 0°$.
- for other current-wave angles is a trend visible that the sediment transport rate will increase when ϕ approaches values of $\phi = 90°$. ($Ss(\phi = 120°) > Ss(\phi = 180°)$ etc.).
- the parameter $a(\phi)$ may be related to the apparent roughness increase parameter $\gamma(\phi)$, a large value of the apparent roughness increase (relative small velocities in the near bed zone), points to a rough bed, which induces high concentrations in the near bed zone and therefore also a large sediment transport rate.

4.7 Ripple parameters

4.7.1 General

Ripples are formed by wave and current movements, yielding a bed form that is specific for the hydraulic conditions at that moment. On the other hand the bed form influences the water movement in the near bed zone, and therefore also the concentrations in the near bed zone.
Here the ripple parameters and the bed forms will be discussed. For each experiment the ripple parameters were determined, in wave and current direction.
During these experiments, with increasing intensity of water movement, the following bed forms occured, defined as:

- 2-dimensional ripples : Regular ripple-shaped bed, (2-D) with ripples in wave-direction.
- 2.5-dimensional ripples : Regular ripples in wave-dir., (2.5-D) also some ripples in current-direction. (Semi-regular ripple-shaped bed.)
- 3-dimensional ripples : Ripples in both directions. A (3-D) "honeycomb-pattern" is present. Irregular ripple shaped bed. (photo 7)

Other forms, like "dunes" or a "flat bed", were not observed in the present study. The bed form for each experiment is listed in the tables with experimental data under "bedf.type:ripples-".

. 2-D ripples were observed only in case of no current, ripples in wave direction.
. 3-D ripples were observed in most of the experiments, clear presency of two ripple directions (see Photo 7)
. 2.5-D ripples were observed for a combination of large wave heights (Hs = 0.10 - 0.14 m) and a weak current (Um = 0.12 m/s)

To describe these ripples, the following parameters are used:

- ripple height (r)
- ripple length (λ)
- ripple steepness (r/λ)
- ripple shape ($\lambda 1/\lambda 2$)

These parameters were determined in the direction of the current and in the direction of the waves. Also the mean values were estimated. These parameters will be described in the next sections.

4.7.2 Bed form asymmetry

In most of the experiments the ripples were asymmetrical. This asymmetry is expressed in the ripple shape. This parameter, the ratio $\lambda 1/\lambda 2$, determines whether the ripples are called wave-dominated (symmetrical) or current-dominated (asymmetrical).
This is sketched in Fig. 16.

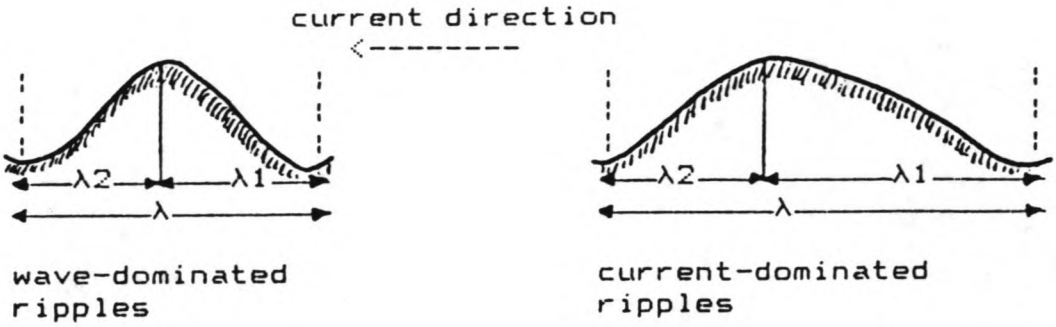

Fig. 16 Wave- and current-dominated ripples

In the present study, $\lambda 1/\lambda 2$-ratio values between 0.85 and 1.3 were found for the ripples in the wave direction. For ripples in current direction the ratio varies between 1.1 and 1.6, with mean values of $(\lambda 1/\lambda 2)_{wave} \approx 1.05$ and $(\lambda 1/\lambda 2)_{current} \approx 1.35$, see Fig. 4.8.A and Table 4.3, 4.4.

The ratio $(\lambda 1/\lambda 2)_{wave}$ is influenced by the wave-direction. For perpendicular waves the ratio $(\lambda 1/\lambda 2)_{wave}$ is independent from the current ripples (and its asymmetry). However, the current ripples influence this ratio for current-wave angles of $\phi = 60°$ and $\phi = 120°$. The ripple-patterns in current and wave direction are interfering each other, so that it is not possible to get "independent" ripple measurements. When determining $(\lambda 1/\lambda 2)_{wave}$ for $\phi = 60°$, the symmetric "wave-ripple" will be influenced by the asymetric "current-ripple". Because of the current-ripples, the wave-ripples become more asymetric (larger $\lambda 1/\lambda 2$-values). The current increases the "upstream wave-length", $\lambda 1$.
For $\phi = 120°$ this influence is also present. Because of the definition (see Section 3.3.7, Fig. 8), the measured $\lambda 1/\lambda 2$-values are, in contradiction to $\phi = 60°$, smaller than normal. In this case the current-ripples increase the "down-wave" ripple length, $\lambda 2$.

To study the influence of the water movement in the near bed zone on the ripple characteristics, the following dimensionless parameters are used:
- $Ub^2/\Delta gD50$, to describe the wave influence,
- $Um^2/\Delta gD50$, to describe the influence of the current strength and
- Um/Ub, to indicate the importance of the current with regard to the waves.

Fig. 4.8.A. shows the relationship between Um/Ub and $\lambda 1/\lambda 2$. One can conclude from this figure that:

. Ripples in current direction are more asymmetrical than ripples in wave direction. This is corresponding with the fact that current-dominated ripples are more asymmetrical than wave-dominated ripples.

. The asymmetry of the current-related ripples is independent of the relative strength of the current and the waves (Um/Ub)

. The asymmetry of the wave-related ripples shows a small increase for increasing Um/Ub-values

4.7.3 Ripple height

The experiments in the present study showed mean ripple heights between 0.62 and 1.37 cm. This range is somewhat below the range that was found for the ripple heights in the earlier 100-mu-study.

The inaccuracy of the ripple height of the 3-D ripples is larger than that of the 2-D ripples, which is caused by the measuring method. More details about this subject are given in Section 5.3.
In Fig. 4.8.B. it is shown that rc ≈ rw , and that there is no influence for Um/Ub.
Fig. 4.8.C. shows the relationship between the parameter rw/Ab, the relative ripple height, and the water movement parameter, $Ub^2/\Delta gD50$.

From this figure it is clear that:

. Increase of Ub leads to decrease of the relative ripple height. (due to erosion at the ripple crest)

. No significant difference is found for the various current-wave angles.

Fig. 4.8.D. shows the relation between rc/h, the relative ripple height in current direction (h = water depth), and the watermovement parameter, $Um^2/\Delta gD50$.

From Fig. 4.8.D. one can see that:

. Increase of Um leads to a small increase of the relative ripple height.

. The increase of the relative ripple height is largest for $\phi = 60°$. For $\phi = 120°$ this increase also seems to be larger than for $\phi = 90°$. The explanation can be that for smaller current-wave angles the turbulence should be lower, (because of the fact that the ripple-pattern is "less 3-D" than for $\phi = 90°$) so that larger ripple heights are more easily formed. This can also explain the fact that the ripple heights formed in the earlier 100-mu-study are somewhat larger. ($\phi = 0°$ and $\phi = 180°$)

4.7.4 Ripple length.

In the present study mean ripple lengths were found of 6 to 11 cm. In the wave direction and the current direction this range is:

$5 \text{ cm} < \lambda w < 12 \text{ cm}$
$7 \text{ cm} < \lambda c < 15 \text{ cm}$

In the earlier 100-mu-study ripple lengths of 6.0 to 14.5 cm were found. Fig. 4.8.B. shows that $\lambda c/\lambda w$ depends on Um/Ub, in contradiction to rc/rw. The ripple lengths are depending on the velocities near the bottom. For increasing velocities the ripple lengths will decrease.
Figs. 4.8.E - F show relationship between the relative ripple lengths, $\lambda w/Ab$ and $\lambda c/h$ and the water movement parameters, $Ub^2/\Delta gD50$ and $Um^2/\Delta gD50$.

From the Figs. 4.8.E - F one can conclude that:

. Increase of wave height leads to a significant decrease of the relative ripple length in wave direction.

. Increase of current strength leads to a small decrease of the relative ripple length in current direction.

. No significant difference in ripple length is found for the various current-wave angles, although the decrease in the ripple length for increasing water movement parameters for $\phi = 120°$ is less clear than for the other current-wave angles.

4.7.5 Ripple steepness

The ripple steepness is defined as the ratio r/λ. This parameter is also determined for wave and current direction.

An average steepness of $r/\lambda = 0.102$ was found in the present study. Further was found $(r/\lambda)c = 0.093$ and $(r/\lambda)w = 0.124$
In the earlier 100-mu-study: $r/\lambda = 0.134$.
From Fig. 4.8.G, no influence of the parameter $Ub^2/\Delta gD50$ on the relative ripple steepness in wave direction was found.
The influence of $Um^2/\Delta gD50$ on the relative ripple steepness in current direction is clear (see Fig. 4.8.H):

. The relative ripple steepness increases for increasing current strength.

. No significant differences are found for the various current-wave angles.

4.8 Size and fall velocity of suspended sediment

In each experiment ten suspended sediment samples were obtained (ten measuring points over the depth). These samples were added together to make a bulk sample. Each bulk sample was analyzed in a settling tube to determine the fall velocity distribution.
The data tables in part F present the measured fall velocity parameters, w50, w10 and w90 of the bulk samples. From these, the particle diameters D10, D50 and D90 can be computed (Ref. Slot,1983).

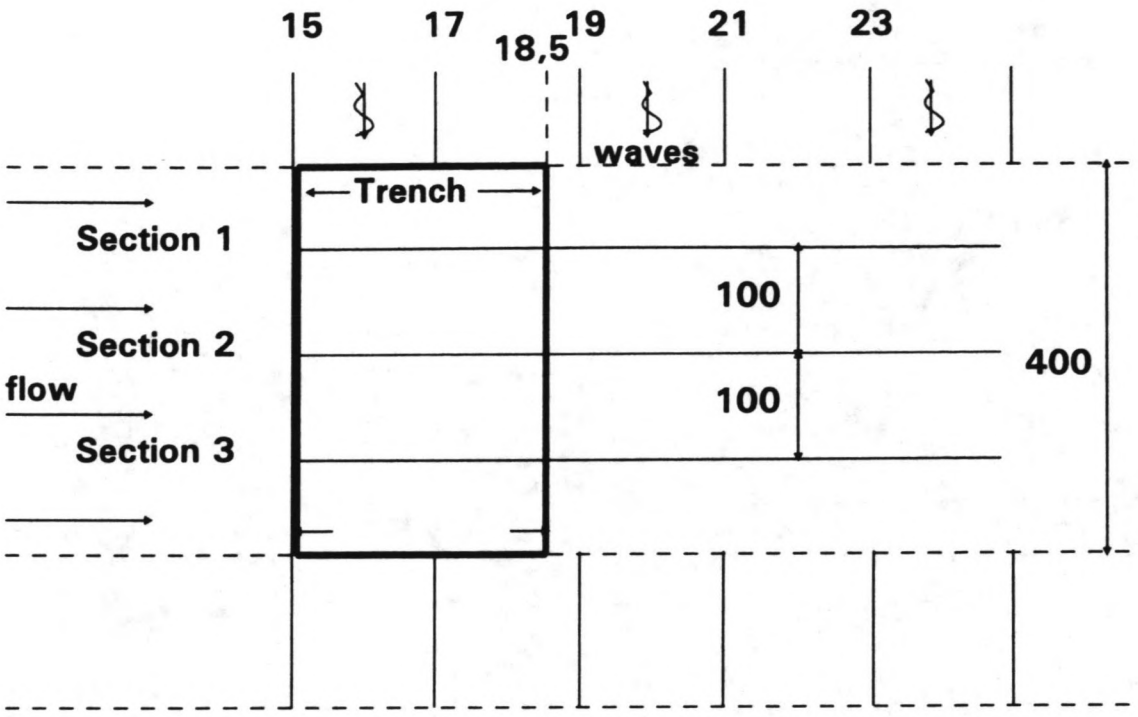

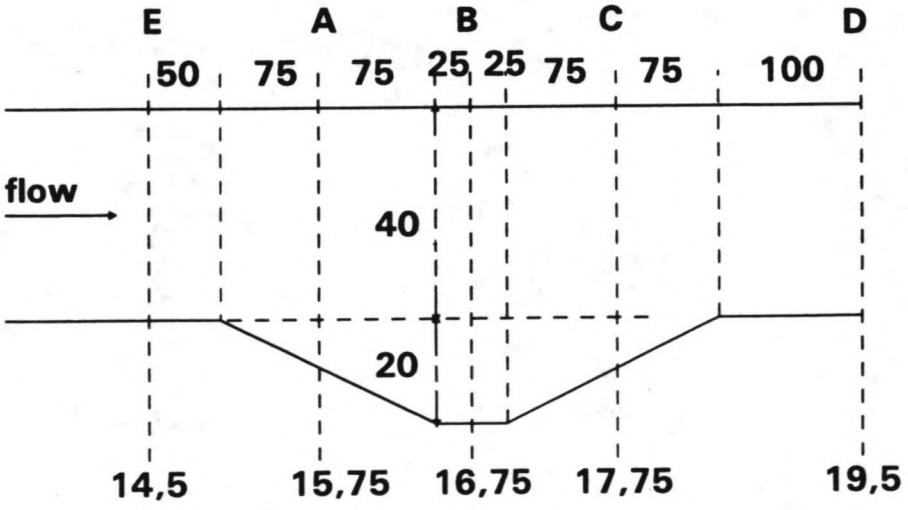

Figure T1 Top and side view of the trench and measuring locations A,B,C,D,E

The results are presented in the Tables 10 and 11:

Wss,x [mm/s]	Wss,10	Wss,50	Wss,90
mean	3.89	6.54	10.82
minimum	3.07	5.41	8.84
maximum	4.27	7.74	12.90

Table 10 Fall velocity parameters

Ds,x [mm]	Ds,10	Ds,50	Ds,90
mean	0.072	0.095	0.123
minimum	0.064	0.086	0.111
maximum	0.078	0.102	0.136

Table 11 Diameter parameters suspended sediment

The differences between the results of the various experiments are relatively small. No clear influence of the wave height and current velocity was observed. The average median particle diameter (d50) of the suspended sediment (95μm) is somewhat smaller than that of the bed material (about 100μm).

4.9 Migration of the trench

In the present study also measurements were carried out in a trench. With the use of a profo the migration of the trench was measured in three sections. The sediment concentrations and velocities were measured along the channel in the sections A - E (see Fig. T1).
The computation method for sediment transports and velocities is the same as for the channel tests.

The purpose of these tests is to compare the results with existing computer models on this subject and to get an insight of the migration of the trench in the time and its relation to the suspended sediment transports along the channel (also time-depending).
The results of the measurements and computations are presented in part F.
The migration of the trench in section 2 is also presented in Fig. T2.

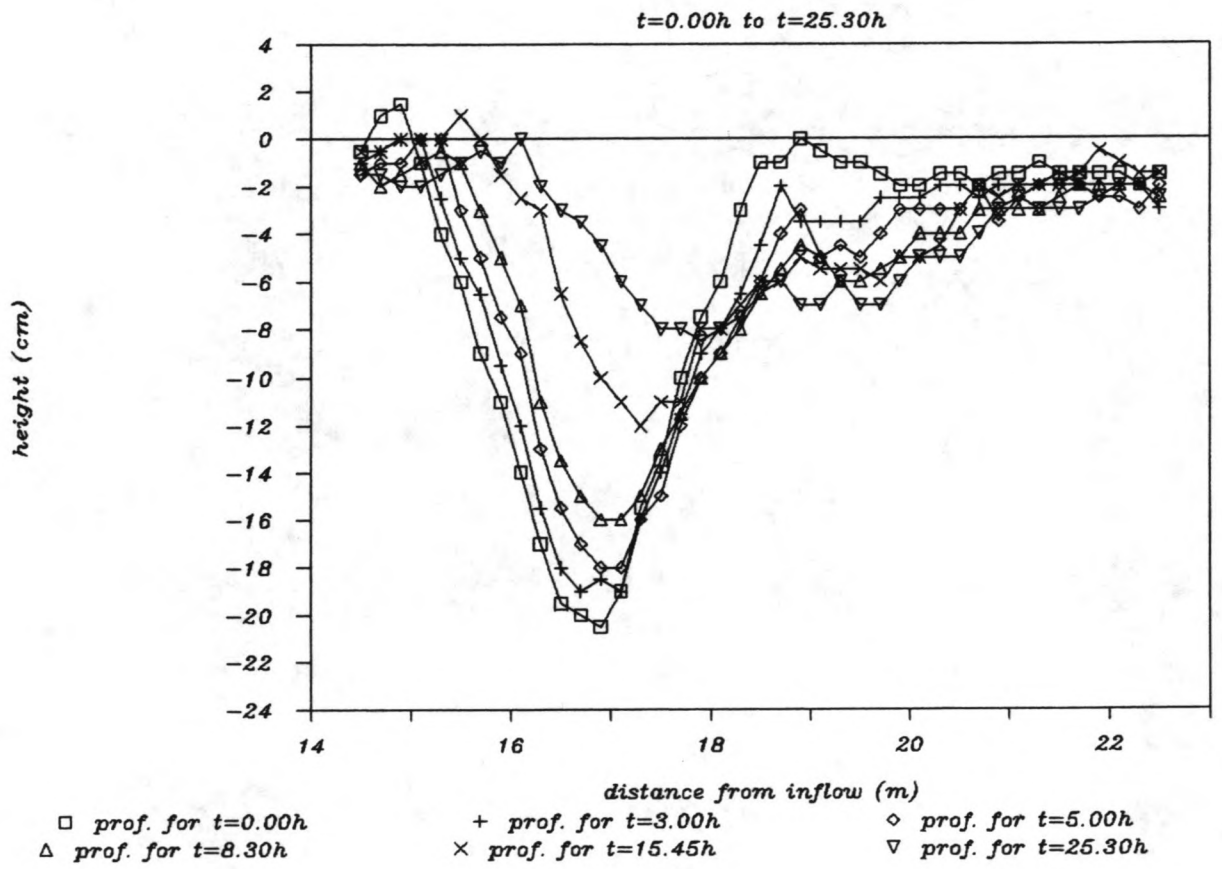

Figure T2 Channel bottom profile Section 2

5. Determination of the bedroughness

5.1 General

In this chapter the bedroughness will be studied. This parameter is related to the shape and size of the ripples and therefore important for the sediment transport rate. According to Jonnson et al (1970), the relationship between the bed shear stress in case of waves alone, and the water velocity near the bed is given by a function which includes a friction factor. This friction factor depends on the water displacement in the near bed zone and the bedroughness. When waves are superimposed on a current, the current profile will change under influence of the waves (see section 4.4.3). In the near bed zone the time-averaged velocity will decrease. This means that the apparent bedroughness increases in case of waves and a current. The zone, where the water motion is noticeably affected by the bed profile, is called the boundary layer.

Rippled type bedforms can change the boundary layer structure in two ways:

- y introducing strong vortices.
  Because of this effect, the boundary layer can extend to aheight far above the bed (several times the ripple height).

- By introducing pressure forces which influence the water motion.

When considering the two effects above, the conclusion is easily drawn that the bedroughness depends highly on the ripple geometry and its configuration. In the next sections the ripple geometry and configuration will be described.

5.2 The ripple geometry

When ripples are formed, they start influencing the water movement. This connection between ripple geometry and the water movement is not well understood in quantitative terms.

The most important ripple characteristics are:

r = ripple height
λ = ripple length
r/λ = ripple steepness

These characteristics can be described in mean values. In case of waves and a current it can be useful to take the asymmetry of the ripples into account. Asymmetric ripples are formed when the current influence on the ripple geometry is relatively large compared to the wave influence. Ripples measured in current direction were **asymmetrical** with $\lambda 1/\lambda 2 \approx 1.35$. Ripples in wave direction were **symmetrical** with $\lambda 1/\lambda 2 \approx 1.05$ (also depending on ϕ).

5.3 The ripple configuration

The ripple heights and the ripple lengths were obtained from measurements (see chapter 3). From these data the ripple steepness was computed as r/λ. If the ripple configuration of the bed is 2-dimensional the ripple geometry can be determined rather accurately. As in the earlier 100 mu-study, a 2-dimensional configuration was only found in case of waves alone. In experiments with a weak current (0.12 m/s) the configuration was 2.5- or 3-dimensional. Increasing the current, only 3-dimensional configurations were found. Because of this effect, the configuration of the ripples in each experiment was noted as :

2 - **D**imensional,
2.5- **D**imensional or
3 - **D**imensional.

This was done by visual observation and comparing ripple lengths in the two directions. ($\lambda c \approx \lambda w$; 3-D configuration).

In case of a 2.5-D configuration the accuracy of the determined ripple parameters will diminish, and a 3-D configuration will diminish the accuracy even more (see Fig. 17).
In case of a 3-dimensional configuration, the larger ripples may have a relatively larger contribution in the bedroughness than the smaller ones (100-mu-study: Nap, Van Kampen, 1988). To get a better accuracy, in the earlier 100-mu-study the parameters Hdom and Ldom were calculated. In these

parameters the individual ripple heights and ripple lengths were weighted with the ripple lengths, so longer ripples gave a relatively larger contribution to Hdom and Ldom.
The result of this computation was that the values of Hdom and Ldom were about 10% larger than the mean values of rm and λm. As is suggested in the earlier 100-mu-study, the accuracy can also be increased by increasing the number of ripple measurements. In the present study the ripple parameters were measured in current and wave direction, so the accuracy of rm and λm will be higher than in the earlier 100-mu-study (more ripple measurements in the present study). The difference between the mean values (rm,λm) and Hdom, Ldom will be smaller than 10% for the present study, so the parameters Hdom, Ldom do not significantly improve the accuracy of the determination of the ripple parameters for the present study. Therefore it was not necessary to compute the parameters Hdom and Ldom for the present study.

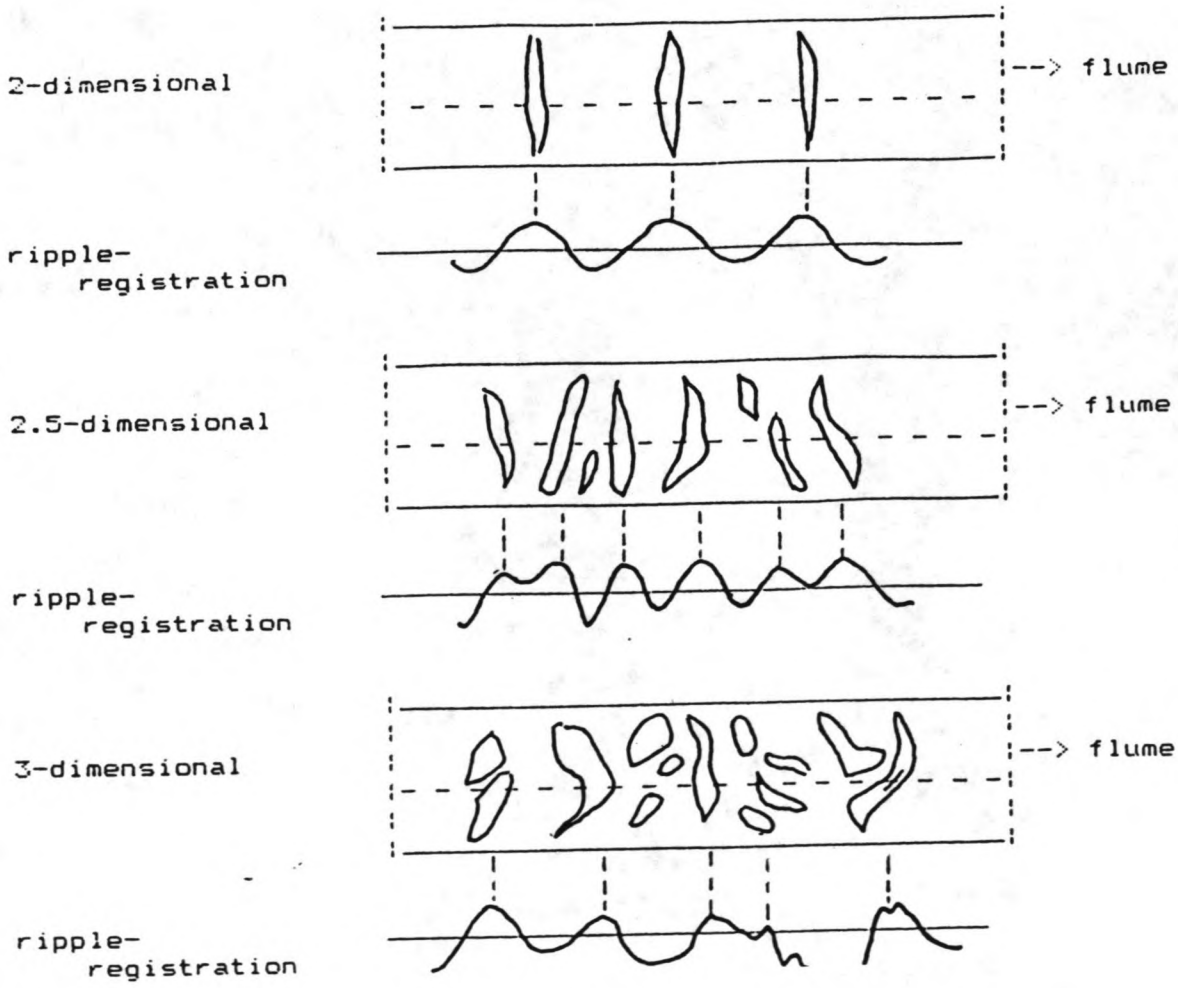

Fig. 17 Effect of the ripple configuration upon the determination of ripple characteristics.

5.4 Determination of the bed roughness

As in the earlier studies, in each experiment the current velocity profile was also measured in absence of waves (see chapter 3). These profiles have been investigated by fitting a logarithmic distribution of the form :

$$U(z) = (U*/\kappa)*\ln(z/z0) \qquad \text{for } z > z0 \tag{5.1}$$

in which:

U(z)	= mean current velocity at height z	[m/s]
U*	= bed shear velocity	[m/s]
z	= height above reference level	[m]
z0	= roughness length scale (zero-vel. level)	[m]
κ	= the Von Karman constant (=0.4)	[-]

(Here it is assumed that the reference level is equal to the mean bed level. In section 5.8 it will be studied whether this assumption is correct.)

The bedroughness can be computed from z0 as :

$$Ks,physical = 33 * z0 \tag{5.2}$$

Using this method, the values of U* and z0 were estimated. For each individual test the velocities of all ten measuring points were calculated using the logarithmic fit. With Eq.(5.2) Ks,phys. can be computed. The highest correlation was always found when all ten points were taken in consideration (see also Figs.5.3.A-I), this in contradiction with the velocity profile for current and waves (see section 5.6).

In the present study, a roughness range (Ks,phys) of 0.1 to 1.5 times the mean ripple height was found. This is true for 76% of the experiments. The mean value is Ks = 0.75 * rm. This doesn't vary much for different ϕ. (see Fig.5.1.A)
In the earlier 100-mu-study, a roughness range, in case of current alone of 3 to 10 times the mean ripple height was found.

When compared to the earlier 100-mu-study the difference in Ks,phys. between the two studies is remarkable. This difference (approximately a factor 10)

may be caused by the influence of the flume walls in the earlier 100-mu-study. Determination via the Vanoni-Brooks method gave in the earlier 100-mu-study a roughness range of 2 to 6 times the mean ripple height. The Vanoni-Brooks method tries to eliminate the influence of the flume walls. The difference is now reduced to a factor of approximately **6**.

5.5 The influence of the ripple steepness

For the ripple steepness, defined as mean ripple height devided by mean ripple length, in the earlier 100-mu-study the following range was found :

$0.10 < r/\lambda < 0.17$

In the present study the range is (see Fig.5.1.B):

$0.07 < r/\lambda < 0.13$

For the ripples in the current and the wave direction this range is:

$0.05 < (r/\lambda)c < 0.14$

$0.08 < (r/\lambda)w < 0.16$

The conclusion made in the earlier 100-mu-study that when $r/\lambda > 0.1$ the influence of the ripple steepness on Ks,phys. becomes less clear, is also found here. For $r/\lambda < 0.1$, the bedroughness parameter Ks,phys. seems to be less than three times the mean ripple height. Further it is remarkable that for flume-studies larger Ks,phys/r-values (Ks,phys/r > 2) were found than for the "channel-studies" (Ks,phys/r < 4). See Fig.5.1.B.

From Fig.5.1.B. the following conclusions can be drawn :

. If the ripple steepness exceeds the value of 0.1, the roughness range varies from 0 to 10 times the ripple height. No significant trend can be observed.

. Within a steepness range of 0.1 to 0.2, a roughness range of 0 to 10 times the ripple height can be expected. For a steepness range of 0.05 to

0.1, the roughness range will be 0 to 3 times the mean ripple height. Within this roughness range, a lower range for relatively coarser (150 μm) sediment and a upper range for relatively finer sediment can be observed.(see Fig.5.1.B)

. The overall roughness range varies from 0 to 5 times the mean ripple height for the "channel" studies. The influence of the side walls in the flume studies is remarkable. In those studies a roughness range of 2 to 12 times the mean ripple is found.

5.6 Roughness prediction for rippled bedforms

Many roughness predictors are available. Most of them are a function of the ripple and sediment characteristics :

$$Ks,phys. = F(r,\lambda,r/\lambda,D50,D90)$$

In the earlier 100- and 200-mu-studies the roughness predictors of Swart, Van Rijn and Grant-Madsen have been used. In the present study only the roughness predictor by Van Rijn was computed for all experiments (see Table 6.1). The predictors are given by the following formulae :

Van Rijn : $Ks,ph. = 3*D90 + 1.1*r*(1-\exp(-25*r/\lambda))$ (5.3)

Swart : $Ks,ph. = 25*((r^2)/\lambda)$ (5.4)

Grant-Madsen : $Ks,ph. = 8*r*(r/\lambda) + 190*D50*\sqrt{t'-0.05}$ (5.5)

in which :

r	= ripple height	[m]
λ	= ripple length	[m]
r/λ	= ripple steepness	[-]
D50	= grain diameter exceeded by 50% of the bed material	[m]
D90	= grain diameter exceeded by 10% of the bed material	[m]
t'	= Shields skin friction parameter (app.IV, Nap,v Kampen)	

As one can see in Table 6.1, the Van Rijn formula gives, for this ripple steepness range, values of Ks,phys. close to 1*rm.

The measured Ks,phys has an average of 0.75*rm. The computed range for Ks,phys./rm :

$1.0 < Ks,phys/rm < 1.10$

with maximum for $r/\lambda=0.126$ and minimum for $r/\lambda=0.075$

"predicted" roughness height

When comparing the roughness range between the present study and the earlier 100-mu-study,the following results were found :

. n the present study (including predictors Swart, Grant-Madsen), a predicted roughness range of 1 to 3 times the mean ripple height was found.

. In the earlier 100-mu-study (also 200-mu-study) a predicted roughness range of 1 to 5 times the mean ripple height was found.

"measured" roughness height

. In the present study a roughness range of 0.1 to 1.5 times the mean ripple height was found.

. In the earlier 100-mu-study a roughness range of 3 to 10 times the mean ripple height was found.

5.7 The wave influence on the bedroughness

The bedroughness range from section 5.6 has been obtained from measurements concerning currents in absence of waves.
The waves will influence the current velocity profile by introducing extra roughness near the bed due to pressure forces. Because of this effect the current profile is shifted.(see Fig.18)
Figure 5.2.A shows that waves superimposed upon a current introduce an apparent roughness, expressed by the factor z1/z0. According to Lundgren (1972) outside a relatively thin layer, the current velocity profile has the usual logarithmic form:

$$U(z) = (U*/\kappa)*\ln(z/z1) \quad \text{for } z > z1 \qquad (5.6)$$

with U(z1) = 0 and Ks,apparent = 33 * z1

The apparent roughness increase is from 33*z0 to 33*z1.
As is shown in the earlier 100-mu-study, the velocity profile is still of a logarithmic form for z > z1. A correlation of 0.98 and higher was only found for z/h < 0.5. In the present study the number of measuring points that gave the highest correlation by fitting to the logarithmic profile, varied from 8 to 10 points; the correlation was always higher than 0.98.

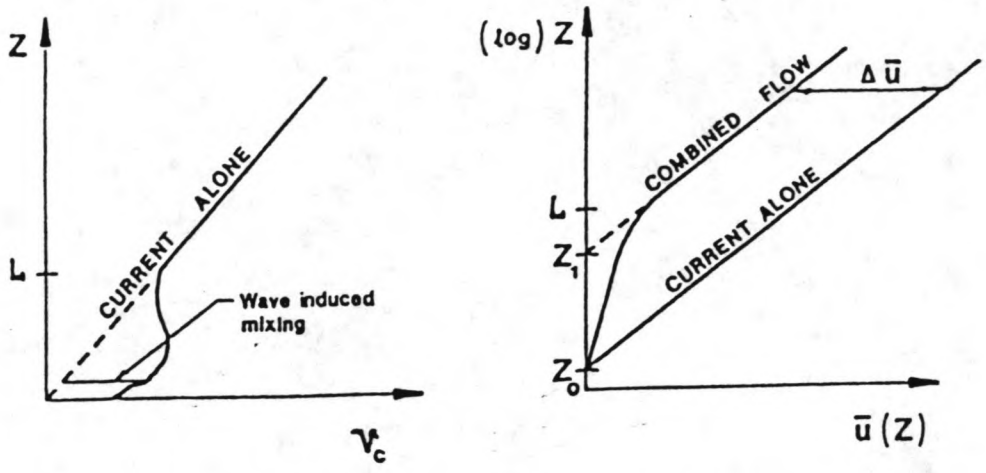

Fig. 18 Apparent roughness increase by wave influence

Based on this curve fitting method, the parameters u* and z1 were determined for all experiments. The apparent roughness increase z1/z0 has been determined too.
An apparent roughness increase of 1 to 30 is found in 88% of the experiments (in the earlier 100-mu-study z1/z0 ≈ 1 to 10). The lower values are found in case of a small significant wave height and a strong current, the higher values in case of a weak current (Um=0.12 m/s), especially for ϕ=90°. It also appears that the z1/z0 values for the experiments T1420-120 and T1430-120 are exceptionally large when compared to the other results. This could be caused by a change in the steering-file of the wave generator. As is described in chapter 3 the waves for these experiments were not reflected via the wall anymore. The consequence was that the velocity measurements were carried out in the section close to the area where waves were absent and hence the velocity profile were relatively uniform.

These experiments are taken out of consideration for further bedroughness analysis.
For the values of Ks,app/rm in the present study, a range is found of 1.5 to 22. The average value of Ks,app here is 5.8 times the mean ripple height. In the earlier 100-mu-study this range was 10 < Ks,app/rm < 56 with an average value of approximately 28. The difference for the roughness in case of current and waves is a factor 5 higher for the earlier 100-mu-study than for the present study. For the roughness in case of current alone this was a factor 10. In the earlier 100-mu-study an average value for Ks,app/Ks,phys(=z1/z0) of 4.3 was found, in the present study the factor was 13.7 (depending on ϕ, see Table 12).

	Ks,app/Ks,phys
ϕ = 0° (earlier 100-mu-study)	3.9
ϕ = 60°	4.7
ϕ = 90°	23.5
ϕ = 120°	12.5
ϕ = 180° (earlier 100-mu-study)	4.6

Table 12 Dependence of Ks,app/Ks,phys on ϕ

From Figure 5.2.A it is clear that Ub/Um is a correct parameter to describe the apparent roughness increase.
According to Van Rijn (1988) Ks,apparent can be described by:

$$Ks,app = Ks,phys. * \exp(\gamma * Ub/Um) \qquad (5.7)$$

The γ-coefficient is dependent on the angle between the current and the waves, as follows :

ϕ = 0° (following waves) : γ = 0.75
ϕ = 180° (opposing waves) : γ = 1.1

In the present study the following γ-values were found (see Table 13)

ϕ	γ (mean)	γ (stand.dev)
90°	2.1	0.9
60°	1.1	0.9
120°	1.7	0.4

Table 13 Dependence γ on ϕ

Considering the large standard deviations one can represent γ roughly by:

$$\gamma = 0.8 + \phi - 0.3\,\phi^2 \qquad (\phi \text{ in radians between } 0 \text{ and } \pi)$$

From these computations the following conclusions can be made :

. In case of irregular waves in combination with a current, an apparent roughness increase of 1 to 30 can be expected. This value varies for different ϕ (less increase for $\phi \neq 90°$), but is significant higher than in the earlier 100-mu-study. For a part this is caused by the low Ks,phys/rm values that were found in the present study.

. As found from the data for the earlier 100-mu-study opposing waves give higher γ-values than following waves. Based on the results it is found : $\gamma 120/\gamma 60 \approx \gamma 180/\gamma 0 = 1.6$. The maximum γ-value is found for $\phi = 90°$. (see Fig. 18).

5.8 Reference level

In this chapter the determination of the bedroughness was discussed. For the computation of Ks,phys and Ks,app the assumption was made that the reference level should be equal to the mean bed level.(see Fig.20)

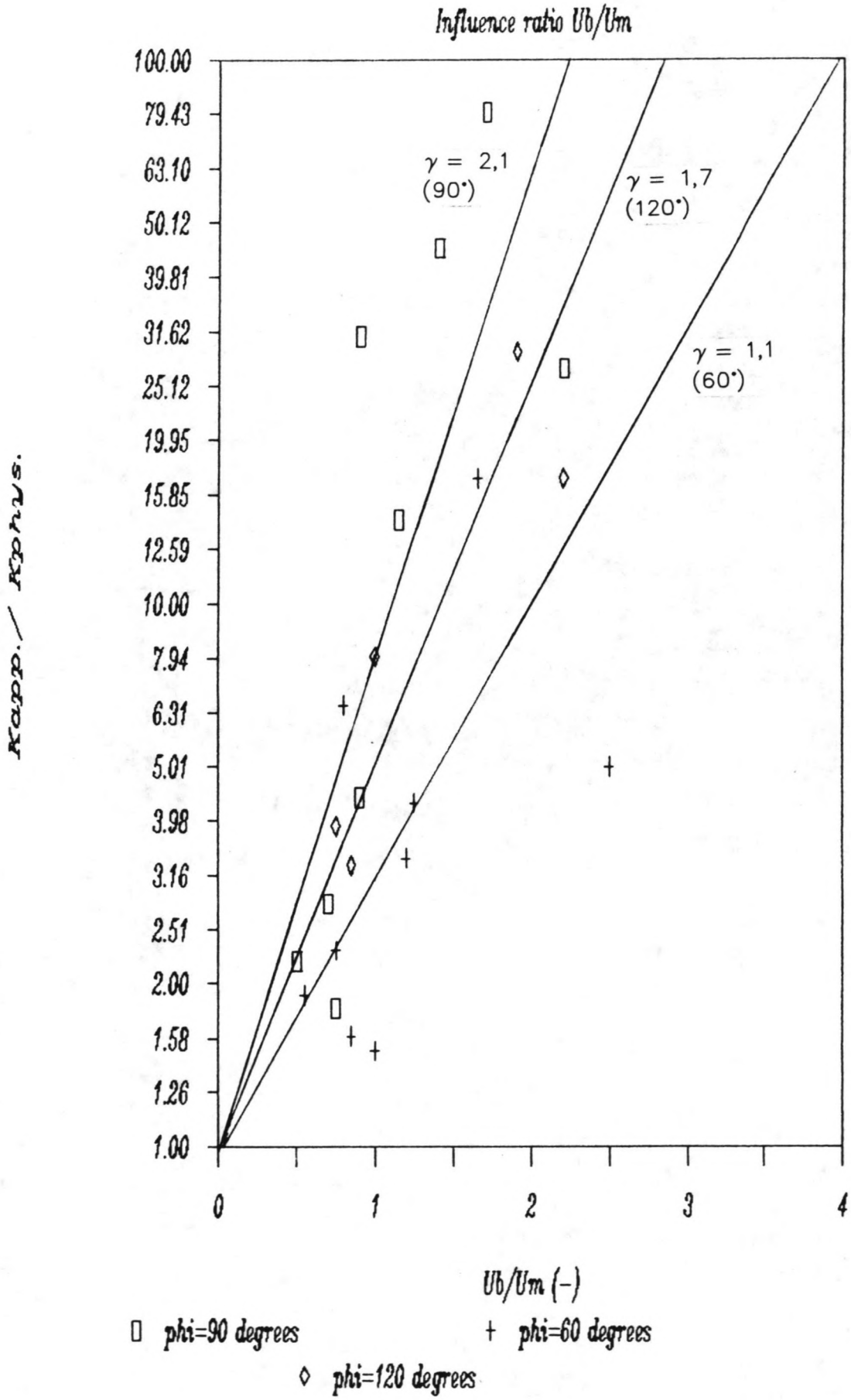

Figure 19 Ratio of $k_{apparent}$ and $k_{physical}$

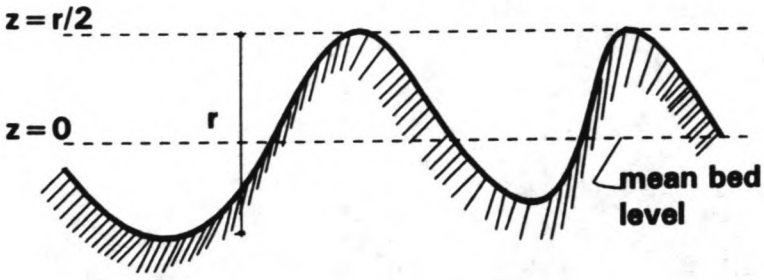

Fig. 20 Mean bed level

In this section the correctness of this assumption is studied. For the experiments with ϕ=90°, the height of the reference level with regard to the mean bed level was computed. For each experiment the height of the reference level was varied. When comparing the measured velocities with a computed logarithmic velocity distribution, an error is made. The overall minimum error for experiments with ϕ=90° is made for Z+ =0.0 cm, so Ks,phys seems to be computed correctly here, although the differences in the added errors are minimal. (see Table 5.3)

However, the influence of the height of the reference level on the bedroughness can be important. When the reference level is situated at half the ripple height below the mean bed level (Z+ ≈ -0.5 cm) , the bedroughness increases with a factor 1.6. The reason for the fact that the reference level could be situated 0.5 cm below the mean bed level is the irregular 3-D pattern of the ripples. It is possible that because of this pattern the current flows "between" the ripples instead of "above" the ripples (see Fig.21).

In this analysis, the reference level is equal to the mean bed level, so this phenomena seems not to be present here, but more investigation could be usefull.

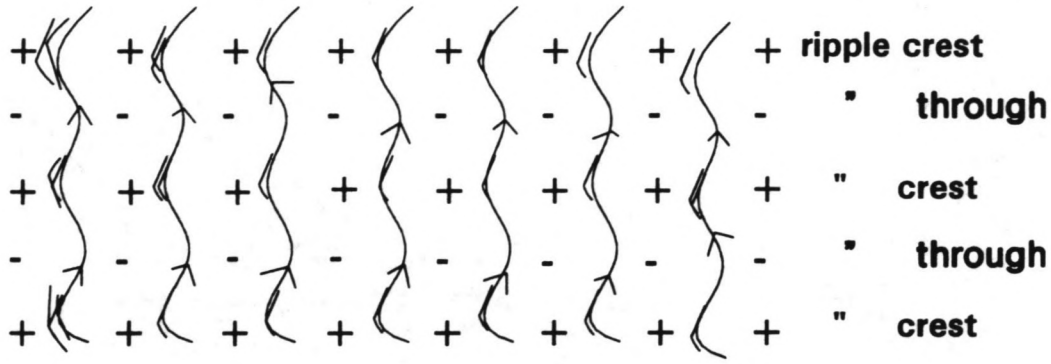

Figure 21A Flow in the near-bed zone for 2-D ripples

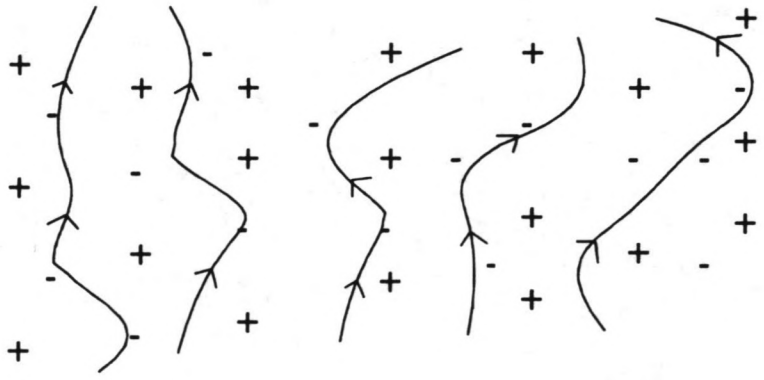

Figure 21B Flow in the near-bed zone for 3-D ripples

6. Models for sediment transport

6.1 General

In this chapter two existing models for sediment transport prediction will be discussed. The models are used to compare the predicted results with the experimental results.

The used models are:

1. Van Rijn model (2nd edition, January 1990)
2. Bijker model (1967,1971). Computer model BAAK (May 1987)

The Bijker model was also used in the earlier 100-mu-study. The Van Rijn model is partly based on the results from that study. Both models give an explicit estimation of the concentration and fluid velocity profiles. The precise description of the formulae are given in Appendix I and II. Their results will be compared to the experimental results. For comparison of the results two classes of transport rates will be distinguished (as in the earlier 100-mu-study): small transport rates (<0.01 kg/ms) and large transport rates (>0.03 kg/ms).

The parameters for calculation of the transport rates will be given in the next paragraph. A precise comparison of formula results and experimental results is not always possible, because the use of the input parameters are subjective. Therefore some assumptions have to be made to accomplish a reasonable comparison.

6.2 Parameters for transport models

6.2.1 General

The parameters, needed for the calculations of transport rates, will be discussed in this paragraph. These parameters are: wave period, wave height and bedroughness. Other parameters, as mean fluid velocity, ripple height and median fall velocity of the sediment, can easily be read from the data tables.

In all computations the following parameters were kept constant:

- mass density of water : $\rho w = 1000$ [kg/m³]
- mass density of sediment : $\rho s = 2650$ [kg/m³]
- porosity : $p = 0.4$ [-]
- acceleration of gravity : $g = 9.81$ [m/s²]
- viscosity : $\nu = 1e\text{-}6$ [m²/s]
- ratio of sediment and fluid mixing coefficient : $\beta = 1.0$ [-]

6.2.2 Wave period

The available parameters for the wave period are:

- The (relative) zero crossing period Tz
- The (relative) wave spectrum peak period Tp,rel

According to the conclusions in the earlier 100-mu-study the use of the relative peak period, Tp,rel, as the characteristic parameter should give the best results, because of the fact that in case of regular waves, the energy wave spectrum shows that most energy is concentrated around this period. To account for the presence of the current, the relative peak period, Tp,rel, and corresponding wave length, L, were used in all computations (see section 4.2.2)

6.2.3 Bedroughness

The bedroughness parameter, Ks, is of great importance for sediment transport computation. For both models three different Ks-values have been chosen:

Van Rijn Model:

1) Ks,w = Ks,c = 3 * rm
2) Ks,w = Ks,c = fit
3) Ks,w = 6 * rm ; Ks,c = 0.75 * rm

with:

Ks,w = wave-related physical roughness height

Ks,c = current-related physical roughness height

fit = roughness determined from logarithmic velocity profile

rm = mean ripple height

Other parameters:

δb = mixing layer = 3 * rm

a = reference level = 0.5 * rm

Bijker Model:

1) Ks = 3 * rm
2) Ks = fit
3) Ks = 0.75 * rm

Case 1) should give the best results when using the Van Rijn Model. Case 2) are the "real" , computed values, and case 3) are the mean values found by curve fitting (see chapter 5).

6.3 Van Rijn formula

For the velocity profile, in the Van Rijn formula a distinction is made for the velocity distribution outside and inside the wave-boundary layer. Outside this layer the velocity distribution is based on the apparent roughness, inside also on the physical roughness. The concentration has a constant value below the reference level, while above this level a concentration gradient is computed.
The Van Rijn formula is based on the time-averaged convection-diffusion equation, with relationships for current-related and wave-related mixing coefficients. The current-related mixing coefficient is described as:

$$\varepsilon_{s,c} = \beta \phi \varepsilon_{f,c} \qquad (6.1)$$

The ϕ-factor in this formula expresses the influence of the sediment particles on the turbulence structure of the fluid (damping effects). Using measured concentration profiles, Van Rijn assumed a concentration-dependent ϕ-factor. For the wave-related sediment mixing coefficient, Van Rijn related

the vertical distribution of the computed sediment mixing coefficient to basic wave parameters. (See Handbook Sediment Transport by currents and waves 2nd edition, by Van Rijn).

A parameter that needs attention in this model is the apparent roughness. This roughness is based on the physical roughness, induced by the current (see chapter 5). For γ, a parameter that describes the apparent roughness increase, Van Rijn proposed lower values (based on experimental data) than the values found in the present study. The apparent roughness increase (especially for ϕ=90°) appears to be higher in the present study. This has its influence on the computed velocities and concentrations.

A comparison between the results from Van Rijn computations with the results from the measurements will now be made.

Sediment transport

From Table 6.1 and Fig.6.5 one can conclude that compared to the experimental data:

- the Van Rijn formula gives good results for Ks,w=Ks,c=3*r, the results for Ks,ph.=0.75*r are moderate, but for Ks=fit the results show less similarity. (see Table 14);

- the computed transport rates in case of a weak current are too small, about a factor 3 for Ks,w=Ks,c=3*r.

	ratio of predicted and measured transport rates	
	small	large
Ks,w=Ks,c=3*r	0.2-1.1	0.9-1.6
Ks,w=Ks,c=fit	0.0-2.5	0.2-3.1
Ks,w=6*r;Ks,c=0.75*r	0.5-2.1	1.4-2.9

Table 14 Ratio of predicted and measured transport rates

Concentration profile

For Ks,w=Ks,c=3*rm the concentration profile is computed and compared with the measured concentration profile (see part F). From the tables and the Figures 6.1,6.2. the following conclusions can be made:

. The concentrations according the Van Rijn Model are too low (about a factor 3) for experiments with a weak current (Um=0.12 m/s). For stronger currents the results are bettter.

. There is no clear trend that the wave height influences the accuracy of the results, this in contradiction to the current strength.

. The steepness of the concentration profile is rather good predicted by the Van Rijn model. A trend is visible that the steepness is somewhat too low for small wave heights and somewhat too high for large wave heights.

6.4 Bijker formula

The Bijker formula is a typical longshore transport formula, based on bed friction forces. The formula only estimates the current-related part of the sediment transport.

The Bijker model computes a total sediment transport, devided in a bed load transport and a suspended load transport. As the bed load transport was not determined in the present study, this part will not be considered now. However for computing the suspended sediment transport, it is necessary to know the concentration in the bed load layer. This concentration can be computed from the bed load transport. The concentration profile is approximated by an Einstein-Rouse concentration distribution, in which the bed layer concentration is used as reference concentration. The velocity profile is assumed to be logarithmic. The suspended load transport follows from multiplication of the concentration and velocity profile. When comparing the measured and computed suspended transports it should be noticed that Bijker defined the suspended transport in the zone from z=Ks to z=h, while the measured suspended sediment is defined between z=1/2*r and z=h.

Some parameters in the Bijker formula need attention, especially the dimensionless empirical parameter B. For this parameter values between 1 and 5 have been suggested. For computation of longshore transport in the breaker-zone this parameter is usually taken equal to 5. In the present study non-breaking waves are involved. Therefore B is chosen equal to 1, as was also done in the earlier studies. Besides this factor gives good results (see Table 6.2). The transition from B=1 to B=5 in relation to the relative wave height Hs/h is unknown.
In the earlier 100-mu-study Ks,phys. had a value of 3 to 7 times the average ripple height. In the present study Ks,phys had a value of 0.1 to 1.5 times the ripple height. The chosen Ks-values are mentioned in section 6.2.

In contradiction to the earlier 100-mu-study the wave height parameter was not varied. The significant wave height was taken for the computation.
Computations have been made for:
- the suspended load transport,
- the concentration distribution.

The results from these computations will now be compared with the results from the measurements.

Sediment transport

Generally spoken one can conclude from Table 6.2 and Fig. 6.5, that compared to the experimental data:

. the Bijker formula gives good results, especially for Ks,phys.=fit and Ks,phys. = mean fit.
. the Bijker formula gives larger transport rates (about a factor 1.5-2 in case of a weak current), but about the same transport rates when increasing the current.

	ratio of predicted and measured transport rates	
	small	large
Ks,w=Ks,c=3*r	1.5-7.8	0.4-0.9
Ks,w=Ks,c=fit	0.5-3.3	0.5-1.0
Ks,w=Ks,c=mean fit	1.0-2.7	0.6-1.0

Table 15 Ratio of predicted and measured transport rates

In the earlier studies larger deviations were found, especially for weak currents. The reason for this can be that Ks,phys in the present study had a value close to half the mean ripple height , the value Bijker suggested. In contradiction with the Van Rijn model, the Ks-values obtained by curve-fitting give very good results from the Bijker model.

Concentration profile

The concentration profile is strongly influenced by the value of the bedroughness parameter, Ks,phys.. The constant concentration between the mean bed level (z=0) and z=Ks,phys. is the reason for this. Because of the fact that Ks,phys. found in the present study is almost equal to the suggested value by Bijker, the results should be better than in the earlier 100-mu-study. The computed bed layer concentration is, compared to the measured concentrations in the near bed zone (see also Figs.6.3,6.4):

- about a factor 3 too large using Ks,ph.=fit,
- about a factor 3 too large using Ks,ph.=mean fit=0.75*rm
- about a factor 5 too large using Ks,ph=3*rm

The concentrations are more comparable than the factors 7 to 12 (too small) found in the earlier 100-mu-study. For the steepness of the concentration profile can be said:

- somewhat higher for Ks,ph.=fit (however very varying results)
- somewhat lower for Ks,ph.=mean fit (also large variations)
- lower for Ks,ph.=3*rm

In the earlier 100-mu-study the concentration profiles according to Bijker were steeper than the measured profiles.

Resuming

The Bijker model gives, generally spoken, good results for B-factor equal to 1.

1. The bedroughness doesn´t influence the model as much as the Van Rijn model, so the three different Ks-values give all reasonable results. The best results were obtained for Ks-values found by curve fitting of the logarithmic velocity profile. For experiments with a weak current, the sediment transport rates are too high. The concentrations in the near bed zone are also too high.

The conclusion for using the Bijker model on the experimental data of the present study:

. The Bijker formula gives good results for strong currents, but too high sediment transport rates in case of a weak current. The concentrations in the near bed zone are somewhat too high.

7. Conclusions and recommendations

Conclusions

1. An increase of the significant wave height or an increase of the depth-averaged fluid velocity leads to an increase of the concentration magnitudes (see 4.3).

2. Largest concentration magnitudes are obtained for a current-wave angle of $\phi=90°$. For $\phi=120°$ and $\phi=60°$ there is no clear difference in the concentration profile (see section 4.3.4).

3. Current in combination with waves have generally smaller velocities in the near bed zone and larger velocities in the upper layers. For a current-wave angle of $\phi=90°$, the velocities in the near bed zone are relatively small, for $\phi=60°$ relatively large. In the upper layers the velocities are relatively large for $\phi=90°$ and relatively small for $\phi=60°$ (see section 4.4.3).

4. The bedroughness parameter, Ks,phys., in case of current alone, is about 0.1 to 1.5 times the mean ripple height (see section 5.6).

5. In case of irregular waves in combination with a current, an apparent roughness increase (Ks,app/Ks,phys.) of 1 to 30 can be expected. The largest increase is for $\phi=90°$, the smallest increase for $\phi=60°$. The apparent roughness Ks,app is about 1.5 to 22 times the mean ripple height.(see section 5.7)

6. The suspended load values in case of waves in combination with a current show an increase for an increase of the significant wave height or the depth-averaged velocity. However, given a constant significant wave height, the suspended load values for waves alone will be larger than for waves in combination with a weak current (0.12 m/s) (see section 4.5.4).

7. The differences in the results of the fall velocity tests of the various experiments are relatively small. No clear influence of the wave height and the current velocity was observed. The average median particle

diameter (d50) of the suspended sediment (95μm) is somewhat smaller than that of the bed material (100 μm) (see section 4.8).

8. The influence of the significant wave height, Hsig, on the suspended load transport, Ss, can be represented rather well by the relationship:

   $Ss \approx Hsig^{q}$

   in which q is a parameter that is related to the depth-averaged fluid velocity.
   The influence of the depth-averaged velocity, Um, on the suspended load transport, Ss, can be reflected by:

   $Ss \approx Um^{y}$

   in which y is a parameter that is related to the significant wave height.

9. The influence of the current-wave angle is represented by the factor $a(\phi)$, a "current-wave-depending" factor for the suspended load transport, Ss. This factor is computed for all experiments and averaged for the various current-wave angles. According to the experimental results largest transports are obtained for $\phi=90°$, and smallest for $\phi=0°$ (see section 4.6).

10. The factor $a(\phi)$ may be related to the parameter $\gamma(\phi)$ (parameter to describe the apparent roughness increase). For both studies, the present study and the earlier 100-mu-study, it appeared that these parameters are small for $\phi=0°$ and $\phi=180°$, and increasing for current-wave angles closer to 90°. A large apparent roughness increase points to relatively low velocities in the near bed zone (rough bed) and therefore high concentrations (see section 4.6, 5.7).

Sediment transport computations:

11. The Van Rijn model predicts reasonably good suspended sediment transport rates for Ks,wav.= Ks,cur.= 3 times the mean ripple height. For Ks=fit and Ks=mean fit the results were less accurate. In case of a weak current the computed transport rates are about a factor three too low. The computed transports are relative sensitive for the bedroughness parameters.

12. The Bijker model predicts reasonably good transport rates for Ks=fit and B-factor equal to 1. The Bijker model predicts too large concentration magnitudes in the near bed zone. In case of a weak current the Bijker model computes transport rates that are a factor 1.5-2 too large. The best results are obtained for Ks=fit (bedroughness determined by curve-fitting).

Recommendations

1. In Determining the bedroughness by means of the water surface slope it is necessary to use several gauging stations over the length of the channel. Determination of the bedroughness by using only two gauging stations, does not give reliable results.

2. The reflection of the waves via the wall must be improved, so that unreflected and reflected waves are less interfering each other and that a more uniform wavepattern is generated. It is not recommended to generate the waves without reflection. (less build up of concentrations).

3. Because of the fact that the ripple pattern influences the concentrations and velocities, the experimental program should be set up with care. Ripples are more easily formed when increasing the current strength or wave height than when these parameters should be decreased. Therefore it is usefull to start the program with small wave heights and a weak current. In the next experiments the wave height and the current strength can be increased. When an experiment should be carried out, that was not planned (for example a repitition test), the waiting period before the experiment should be relatively long (at least an hour).

4. The only way to calibrate the E.M.S. is to calibrate at still water. Other methods were not reliable.

5. Attention should be paid to the set up of the measuring carriage. The E.M.S. and the A.S.T.M. should not be placed in the wake of eachother.

REFERENCES

Battjes, J.A. (1982)
"Windgolven"
Lecture notes
Delft University of Technology

Bosman, J.J. (1982)
"Concentration measurements under oscillating water motion"
Report on model investigation (M1965-II)
Delft Hydraulics Laboratory

Bosman, J.J. (1985)
"Concentration measurements in model and prototype"
Concept
Delft Hydraulics Laboratory

Bosman, J.J.; Velden, E.T.J.M. van der; Hulsbergen C.H. (1987)
"Sediment concentration measurements by transverse suction"
Published in ´Coastal engineering´ ,december 1987

Jonsson, I.G. ; Skougaard, Ch.; Wang, J.D. (1970)
"Interaction between waves currents"
Proceedings of the twelfth Coastal Engineering Conference chapter 30, page 489-508

Kaay, Th. van der; Nieuwjaar, M.W.C. (1987)
"Sediment concentrations and sediment transport in case of irregular non-breaking waves with a current"
Report
Delft University of Technology

Kampen, H.F.A. van; Nap, E.N. (1988)
"Sediment concentrations and sediment transport in case of irregular non-breaking waves with a current"
Report
Delft University of Technology

REFERENCES (continued)

Rijn, L.C. van (1986)
"Data Base Sediment Transport"
Report H186-04
Delft Hydraulics Laboratory

Rijn, L.C. van (1990)
"Handbook Sediment Transport by currents and waves, 2nd edition"
Report
Delft Hydraulics Laboratory

delft hydraulics

main office
Rotterdamseweg 185
p.o. box 177
2600 MH Delft
The Netherlands
telephone (31) 15 - 56 93 53
telefax (31) 15 - 61 96 74
telex 38176 hydel-nl

location ' De Voorst '
Voorsterweg 28, Marknesse
p.o. box 152
8300 AD Emmeloord
The Netherlands
telephone (31) 5274 - 29 22
telefax (31) 5274 - 35 73
telex 42290 hylvo-nl